Insights Into the Crustal-Scale Dynamics of a Doubly Vergent Orogen From a Quantitative Analysis of Its Forelands: A Case Study of the Eastern Pyrenees

Arjan R. Grool, Mary Ford, Jaume Vergés, Ritske S. Huismans, Frédéric Christophoul, Armin Dielforder

AGU PUBLICATIONS

Tectonics

RESEARCH ARTICLE
10.1002/2017TC004731

Key Points:
- Cross-section restoration reveals ~111 km minimum shortening in the Eastern Pyrenees, excluding closure of an exhumed mantle domain
- The shortening distribution between pro and retro evolved from roughly equal during rift inversion to pro-dominant during main collision
- This change in shortening distribution from equal to pro-dominant may be intrinsic to all inverted rift systems

Supporting Information:
- Supporting Information S1
- Data Set S1
- Data Set S2

Correspondence to:
A. R. Grool,
agrool@crpg.cnrs-nancy.fr

Citation:
Grool, A. R., Ford, M., Vergés, J., Huismans, R. S., Christophoul, F., & Dielforder, A. (2018). Insights into the crustal-scale dynamics of a doubly vergent orogen from a quantitative analysis of its forelands: A case study of the Eastern Pyrenees. *Tectonics*, *37*, 450–476. https://doi.org/10.1002/2017TC004731

Received 20 JUL 2017
Accepted 26 DEC 2017
Accepted article online 15 JAN 2018
Published online 8 FEB 2018

Insights Into the Crustal-Scale Dynamics of a Doubly Vergent Orogen From a Quantitative Analysis of Its Forelands: A Case Study of the Eastern Pyrenees

Arjan R. Grool[1,2], Mary Ford[1], Jaume Vergés[3], Ritske S. Huismans[2], Frédéric Christophoul[4], and Armin Dielforder[1,5]

[1]CRPG, UMR 7358, Vandœuvre-lès-Nancy, France, [2]Department of Earth Sciences, University of Bergen, Bergen, Norway, [3]Institute of Earth Sciences Jaume Almera (ICTJA), CSIC, Barcelona, Spain, [4]GET, UMR 5563, Université de Toulouse-CNRS-IRD-OMP, Toulouse, France, [5]GFZ German Research Centre for Geosciences, Helmholz Centre Potsdam, Potsdam, Germany

Abstract In natural doubly vergent orogens, the relationship between the pro- and retro-wedges is, as yet, poorly constrained. We present a detailed tectonostratigraphic study of the retro-wedge of the Eastern Pyrenees (Europe) and link its evolution to that of the pro-wedge (Iberia) in order to derive insight into the crustal-scale dynamics of doubly vergent orogens. Based on cross-section restoration and subsidence analyses, we divide the East Pyrenean evolution into four phases. The first phase (Late Cretaceous) is characterized by closure of an exhumed mantle domain between the Iberian and European plates and inversion of a salt-rich, thermally unequilibrated rift system. Overall shortening (~1 mm/yr) was distributed roughly equally between both margins over some 20 Myr. A quiescent phase (Paleocene) was apparently restricted to the retro-wedge with slow, continuous deformation in the pro-wedge (~0.4 mm/yr). This phase occurred between closure of the exhumed mantle domain and onset of main collision. The main collision phase (Eocene) records the highest shortening rate (~3.1 mm/yr), which was predominantly accommodated in the pro-wedge. During the final phase (Oligocene), the retro-wedge was apparently inactive, and shortening of the pro-wedge slowed (~2.2 mm/yr). Minimum total shortening of the Eastern Pyrenees is ~111 km, excluding closure of the exhumed mantle domain. The retro-wedge accommodated ~20 km of shortening. The shortening distribution between the pro- and retro-wedges evolved from roughly equal during rift inversion to pro-dominant during main collision. This change in shortening distribution may be intrinsic to all inverted rift systems.

1. Introduction

It is common in foreland basin modeling and fold-and-thrust belt studies to analyze only one side of a doubly vergent orogen (e.g., Decarlis et al., 2014; Ershov et al., 2003; Fillon et al., 2013). However, several studies, mainly based on mechanical modeling, suggest that pro- and retro-wedges interact in accommodating plate convergence (Erdős et al., 2015; Hoth et al., 2007, 2008; Sinclair et al., 2005; Willett et al., 1993). Correlating the behavior of the two wedges in doubly vergent orogens can therefore provide important insight into orogen dynamics. How deformation and subsidence of the pro- and retro-wedges and -forelands of a natural system relate to each other, whether this relationship changes through time, and what would cause such a change remain unclear. Detailed comparisons of the two wedges and their foreland basins in terms of structure and evolution are required to investigate these issues.

In this paper we investigate the Eastern Pyrenees, comparing and correlating the northern retro-wedge and southern pro-wedge along two sections directly opposite each other to better understand full orogen evolution (Figure 1). The South Pyrenean fold-and-thrust belt and Ebro foreland basin system is extremely well documented owing to excellent outcrop conditions and well-defined stratigraphy (e.g., Burbank, Puigdefàbregas, et al., 1992; Gómez-Paccard et al., 2012; López-Blanco et al., 2000; Vergés et al., 1992). It developed on the subducting Iberian plate starting in the Late Cretaceous. Subsidence records show locally short-lived and accelerating subsidence owing to constant outward basin migration and incorporation of the proximal basin into the thrust wedge. This corresponds to the simulated behavior of kinematic and mechanical models of pro-forelands (Beaumont et al., 2000; Erdős et al., 2014; Fillon et al., 2013; Naylor & Sinclair, 2008; Sinclair & Naylor, 2012). In contrast, owing to poorer outcrop conditions and structural and stratigraphic complexity, our understanding of the North Pyrenean

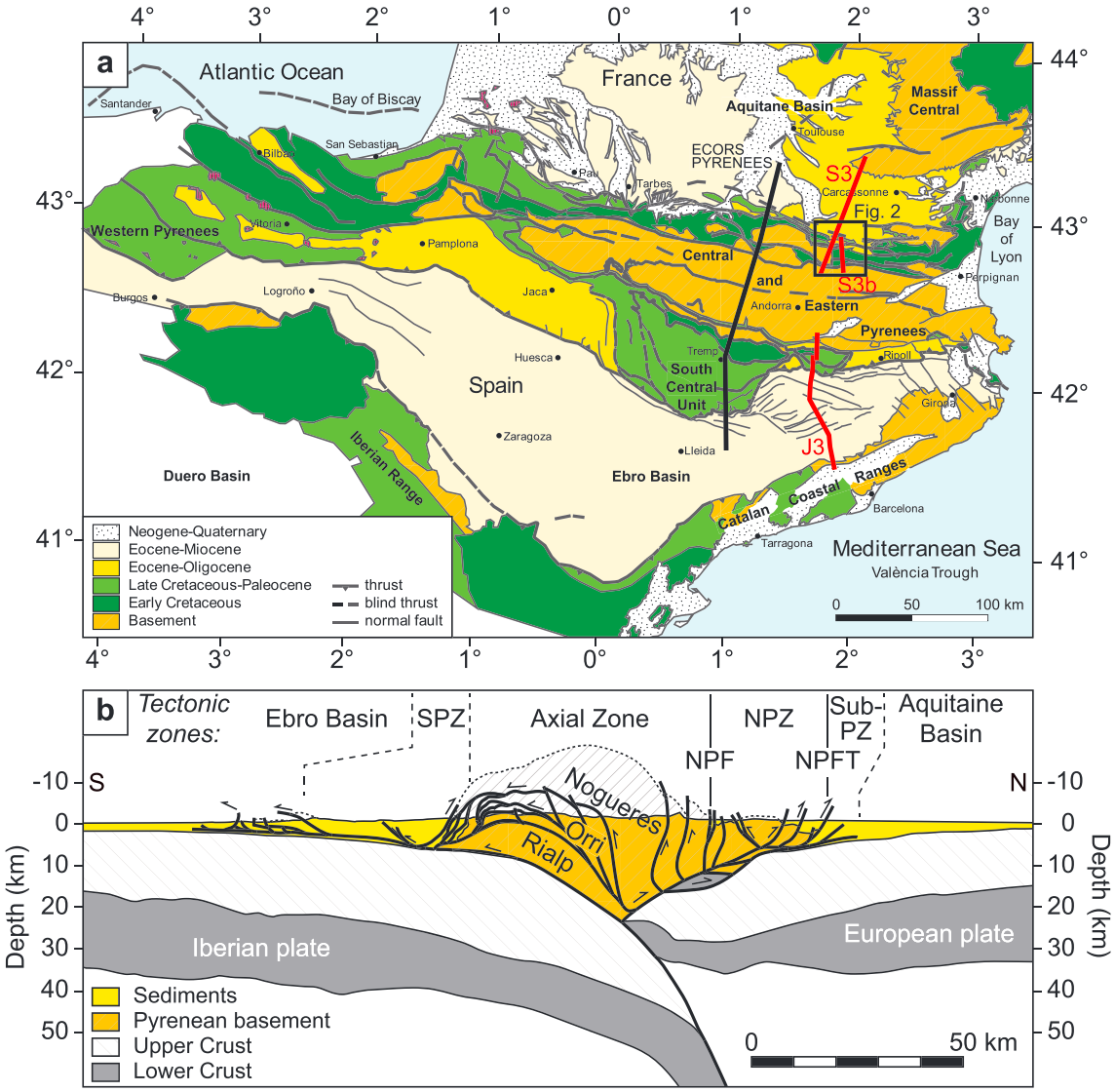

Figure 1. (a) Simplified geologic map of the Pyrenees. Red lines locate the cross sections (Figures 4, 5, and 9). Black line indicates the trace of the ECORS Pyrenees deep seismic section shown in Figure 1b. Modified after Vergés et al. (2002) and Angrand et al. (2018). (b) Interpretation of the ECORS Pyrenees deep seismic section, with major structural zones indicated. Modified after Muñoz (1992). SPZ, South Pyrenean Zone; NPZ, North Pyrenean Zone; Sub-PZ, sub Pyrenean Zone; NPF, North Pyrenean Fault; NPFT, North Pyrenean Frontal Thrust.

retro-wedge is less well developed despite a large body of work spanning several decades (e.g., Choukroune, 1974; Clerc et al., 2015; Lagabrielle et al., 2010; Puigdefàbregas & Souquet, 1986; Souquet et al., 1977). The retro-wedge preserves an inverted hyper-extended rift system of Early Cretaceous age, as recorded by the presence of mantle blocks and syn-extension high-temperature metamorphism in the internal, southern part of the retro-wedge (Clerc et al., 2015; Jammes et al., 2009; Lagabrielle et al., 2010; Mouthereau et al., 2014; Vacherat et al., 2016). In general, retro-wedges can be expected to accommodate less shortening than pro-wedges, resulting in slow and long-lived foreland basin subsidence (Sinclair & Naylor, 2012). Previous work proposes that the western Aquitaine Basin follows this predicted pattern (Desegaulx & Brunet, 1990; Naylor & Sinclair, 2008); however, more recent work shows that the eastern retro-foreland basin has a more complex history that challenges these models, including a temporary stagnation in subsidence for which the cause remains unclear (Ford et al., 2016; Rougier et al., 2016).

To be able to make a detailed comparison of the pro- and retro-wedges and -forelands, we studied the tectonic and stratigraphic evolution of the North Pyrenean Zone and Aquitaine foreland basin in the Eastern Pyrenees (Ariège, France; Figure 1). Our work is based on a structural analysis and cross-section balancing that integrated newly acquired field data, seismic reflection profiles, borehole data, and published stratigraphic and structural data (e.g., Baby, 1988; Bilotte, Cosson, et al., 1988; Choukroune, 1974). This allowed us to decipher the geometry, timing, rates, and kinematics of deformation and to identify and characterize the various phases, styles, and amounts of Santonian to Oligocene shortening in the eastern Pyrenean retro-wedge and its foreland basin. We then correlated this complete retro-wedge history with its pro-wedge counterpart in the Spanish Pyrenees using the works of Vergés (1993), Vergés et al. (1995, 1998, 2002), and Vergés and García-Senz (2001). We identified key differences and point out possible interactions between the pro- and retro-foreland fold belts. Then, we investigate how shortening was partitioned in time and space between the pro- and retro-wedges and discuss what controls the sequence of deformation during orogeny by presenting a new crustal-scale model for the evolution of the Eastern Pyrenees.

2. Geological Setting

2.1. Plate Kinematics

The Pyrenees formed as part of the Alpine belt due to the collision of the Iberian microplate with the European continent. Before the collision, an Aptian to early Cenomanian oblique rift system associated with exhumation of mantle rocks formed between the two plates (Debroas, 1990; Jammes et al., 2009; Lagabrielle et al., 2010). Rifting has been related to the opening North Atlantic Ocean (Olivet, 1996; Sibuet et al., 2004; Srivastava et al., 1990). No consensus on plate kinematics around Iberia yet exists, and there are several competing models. Most models are based on reconstructions of magnetic seafloor anomalies of the Bay of Biscay, Central, and North Atlantic Ocean (Olivet, 1996; Sibuet et al., 2004; Vissers & Meijer, 2012a, 2012b). These models predict different extensional histories for the Pyrenean realm and, after the onset of convergence (~84 Ma), predict different degrees of obliquity for N-S shortening. Pyrenean tectonic structures predominantly record a N-S shortening direction and a minor strike-slip component that was mainly focused along the North Pyrenean Fault (Choukroune & Mattauer, 1978; Souquet et al., 1977).

2.2. Tectonic Zones and Major Boundaries

In the Eastern Pyrenees, the orogen is divided into six tectonostratigraphic zones (Figure 1b). From north to south, the Aquitaine foreland basin is followed by the sub Pyrenean Zone, a folded and faulted zone north of the North Pyrenean Frontal Thrust, usually delimited by a blind thrust (Ford et al., 2016; Rougier et al., 2016; Souquet et al., 1977). South of the North Pyrenean Frontal Thrust is the North Pyrenean Zone, a narrow, north verging fold-and-thrust belt. In the study area, this zone consists of inverted rift basins (e.g., Fougax and Roquefeuil blocks; Figure 2), inverted basement massifs (e.g., Saint-Barthélémy Massif; Figure 2), and the Metamorphic Internal Zone (Figure 2; Souquet et al., 1977). The North Pyrenean Fault separates the North Pyrenean Zone from the Axial Zone and is traditionally seen as the suture between Europe and Iberia. In the classic interpretation of the ECORS section lying some 50 km to the west (see below; e.g., Muñoz, 1992), crustal thickening in the Axial Zone is related to a south verging, antiformal stack of Iberian crust. Interpretations in the Eastern and Western Pyrenees show almost no Alpine folding of Paleozoic basement rocks of the Axial Zone (Teixell et al., 2016; Vergés et al., 2002). South of the Axial Zone lies the South Pyrenean Zone, a south verging thin-skinned fold-and-thrust belt with syn-orogenic thrust sheet-top basins. The Ebro Basin forms the pro-foreland basin of the Pyrenees. It is an asymmetric double flexural basin with a central intrabasinal high due to loading by the Pyrenees in the north and the Catalan Coastal Ranges in the south.

The deep crustal structure of the Central Pyrenees is imaged by the ECORS Pyrenees deep seismic study (Figure 1b; Muñoz, 1992; Roure et al., 1989; Roure & Choukroune, 1998) and more recently by seismic tomography studies (Chevrot et al., 2015; Souriau et al., 2008; Wang et al., 2016). These data show the Iberian Moho underthrusting the European plate, deepening northward from 35 km to 50 km depth (Beaumont et al., 2000). Most authors show the European Moho at a fairly constant 30 km depth along the ECORS line (Beaumont et al., 2000; Díaz & Gallart, 2009), and some show a gentle southward dip (Roure et al., 1989; Roure & Choukroune, 1998). Recent seismic tomography data show the subduction interface dipping 20° northward and show the European Moho rising southward (Chevrot et al., 2015).

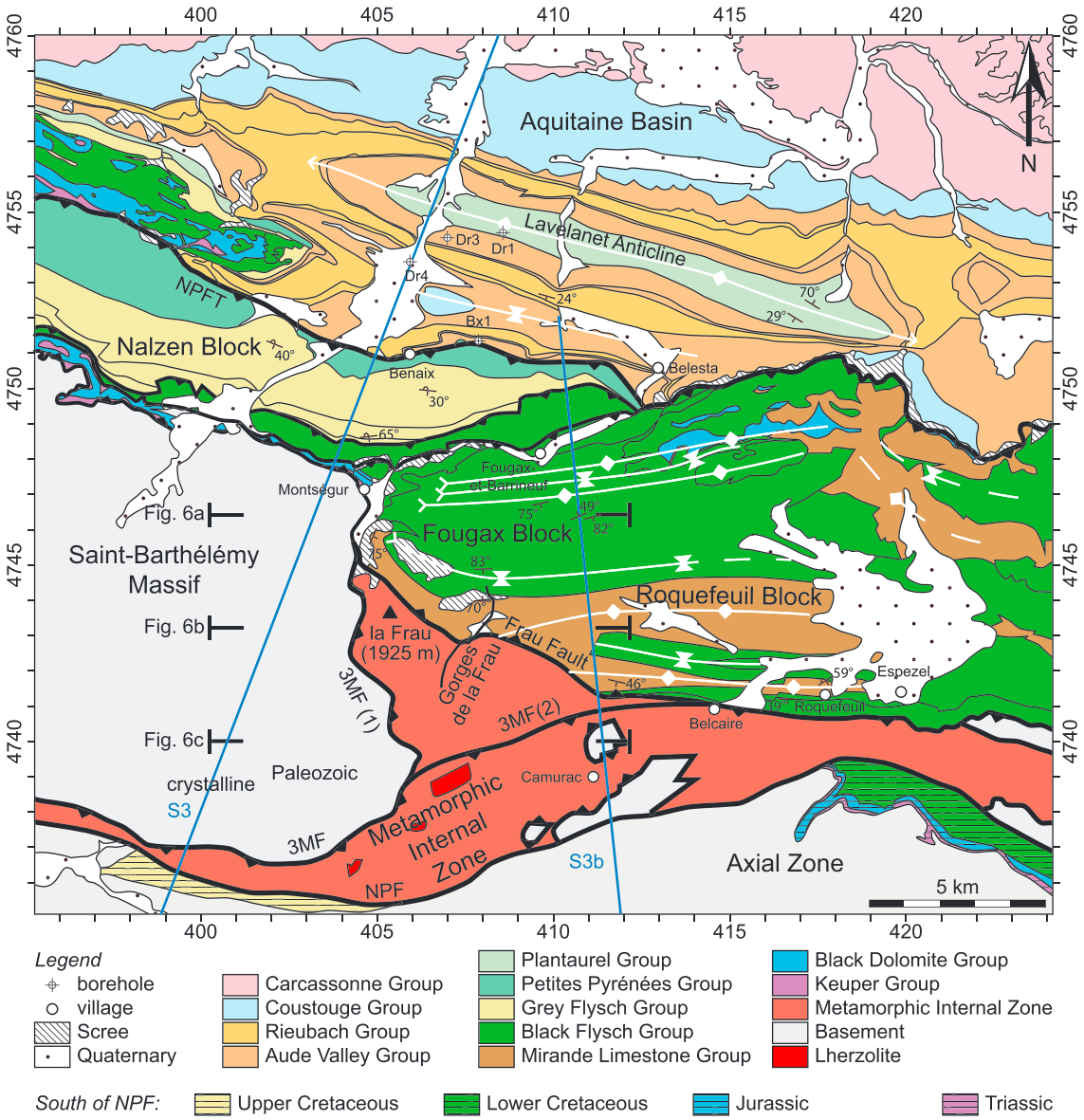

Figure 2. Geologic map of the North Pyrenean Zone and sub Pyrenean Zone, compiled from the BRGM 1:50,000 geologic maps (1075 Foix and 1076 Lavelanet), Marty (1976), and de Saint Blanquat et al. (2016). Boreholes are located between the North Pyrenean Frontal Thrust and the Lavelanet Anticline. The blue lines indicate partial section traces of S3 and S3b. NPFT, North Pyrenean Frontal Thrust; 3MF, 3M Fault; 3MF(1), flat of 3M Fault; 3MF(2), hanging wall shortcut of 3M Fault; NPF, North Pyrenean Fault.

The nature and extent of Alpine deformation in the Axial Zone and the role of inherited Variscan shear zones are currently subject to renewed debate and analysis with modern tools (e.g., Cochelin et al., 2017; Laumonier, 2015). In this paper we focus on the fold-and-thrust belts and foreland basins on both sides of the Eastern Pyrenees. As a detailed analysis of the Axial Zone is beyond the scope of this paper, we use the Axial Zone model of Vergés et al. (1995, 2002) and Vergés and García-Senz (2001), which remains valid.

3. Methods

In order to investigate the structural evolution of the retro-wedge, we constructed two cross sections, the main section S3 and an auxiliary section S3b (for location, see Figures 1a and 2). These sections were positioned directly opposite cross section J3 of Vergés (1993) in the pro-wedge. Standard balancing techniques were used to restore the sections (Woodward et al., 1989). While most sedimentary strata were line-length

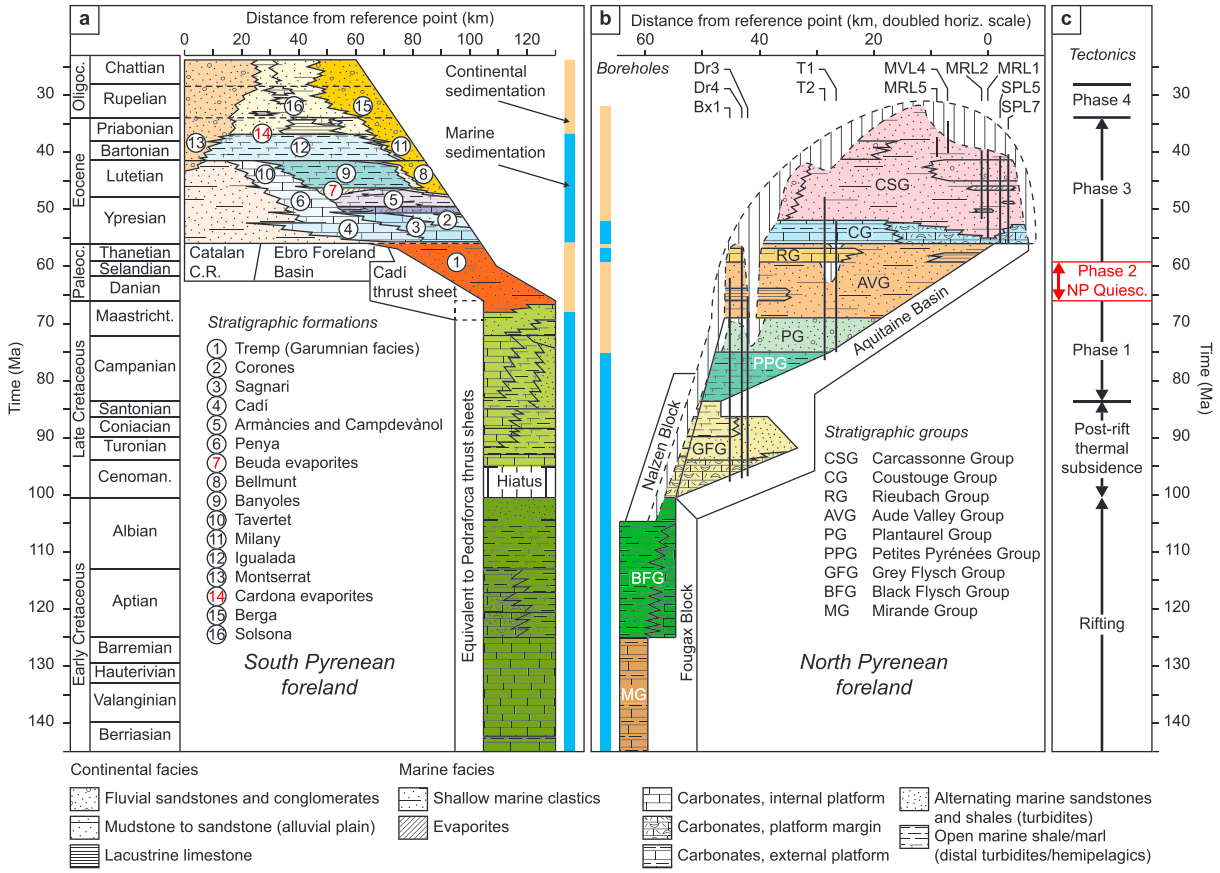

Figure 3. Chronostratigraphic charts for the North and South Pyrenean foreland basins. (a) South Pyrenean stratigraphic chart modified after Vergés (1993) and Vergés et al. (2002). (b) North Pyrenean stratigraphic chart. Boreholes Dr3, Dr4, and Bx1 are located in Figure 2. Note double horizontal scaling compared to Figure 3a. For detailed north Pyrenean formation names and BRGM unit codes, see Table A1. (c) Timing of main tectonic events. Phases 1 to 4 represent the Pyrenean orogeny.

balanced, weak units with significant internal deformation were also area balanced. We used the restored cross sections combined with stratigraphic constraints on timing of activity to estimate average shortening rates for each map-scale structure across the pro- and retro-wedges of the Eastern Pyrenees. The minimum overall shortening rate for a given period was derived by summing the shortening rates for all unlinked structures active during that period. A complete high resolution shortening history across the whole orogen can thus be constructed. Such an analysis integrating detailed map-scale structural history is especially important in areas that record very slow and distributed shortening like the Pyrenees. This shortening history was then used to constrain the crustal-scale restoration model, together with subsidence histories, thermochronology data, and deep geophysical data.

The retro-foreland database includes surface geology from 1:50,000 geological maps of the French Geological Survey (BRGM; 1036 Castelnaudary (Cavaillé et al., 1975a), 1058 Mirepoix (Cavaillé, 1976a), 1075 Foix (Bilotte, Casteras, et al., 1988), and 1076 Lavelanet (Bilotte, Cosson, et al., 1988)), an unpublished geological map (Marty, 1976), publicly available borehole data (Bureau Exploration-Production des Hydrocarbures; now minergies.fr), limited seismic reflection data provided by the BRGM, a 90 m SRTM Digital Elevation Model processed and distributed by the Consortium for Spatial Information (CGIAR) (srtm.csi.cgiar.org; Jarvis et al., 2008), and our own field data. The stratigraphic framework used for the retro-foreland was established by the ANR PYRAMID research project (Ford et al., 2016; Rougier et al., 2016) and linked to the 2013/01 chronostratigraphic chart published by the International Commission on Stratigraphy (Cohen et al., 2013). Details on stratigraphic nomenclature and equivalent BRGM units are presented in Table A1 (in the supplementary information). The lithostratigraphy and chronostratigraphy for the pro-foreland are based on Vergés (1993) and Vergés et al. (1998, 2002).

Total and tectonic subsidence curves for four wells in the retro-foreland are compared with those for six wells or sections in the pro-foreland (Vergés et al., 1998), all calibrated to present-day sea level. We used standard methods of decompaction and backstripping assuming Airy isostasy (Steckler & Watts, 1978). Decompaction calculations integrate the values for initial porosity φ_0 and compaction coefficient c for each lithology as used in Vergés et al. (1998). For the backstripping process, each unit was given bulk values for those constants based on the percentages of each lithology in that particular unit (Table A2). These percentages were determined from the highest resolution sections available, ranging in scale between 1:500 and 1:2,000. Estimates for paleobathymetry were based on depositional environments. Continental deposits were considered to be equivalent to water-filled basins with 0 or −50 m bathymetry. We used a mantle density of 3,300 kg/m^3 and a density of 1,000 kg/m^3 for water. The original published subsidence calculations for the pro-foreland did not take into account eustatic sea level changes (Vergés et al., 1998). These data were therefore converted using the same eustatic data as used for the retro-foreland (Snedden & Liu, 2010). In displaying total and tectonic subsidence relative to present-day sea level, many curves start above 0 m because paleo-sea level was between 160 and 210 m higher than present day and paleo-bathymetry in the forelands was relatively minor. In the case of the pro-foreland, including the long-term eustatic sea level curve may introduce artifacts in the subsidence. Brief periods of low bathymetry in the Eocene are shown as tectonic uplift events in our converted curves, but the observed reduction in bathymetry may have been caused by a short-lived deviation from the long-term sea level curve instead (Burbank, Puigdefàbregas, et al., 1992). Errors in the estimation of bathymetry have the greatest effect on calculated subsidence. Errors in sea level and sediment ages have less impact.

4. North Pyrenean Foreland

4.1. Stratigraphy of the North Pyrenean Foreland

Across the Saint-Barthélémy-Fougax study area, a Mesozoic to Cenozoic succession overlies Variscan basement, which consists of Paleozoic metasediments and crystalline rocks (Figure 3b). Triassic to lower Cenomanian marine strata record rift-related subsidence. Upper Cenomanian to Santonian strata record post-rift subsidence. On a regional scale, the syn-orogenic succession (Campanian to Oligocene) records a consistent along-strike transition from continental to marine facies to the west with facies interfingering in the study area. No strata older than Cenomanian overlie Variscan basement north of the Benaix Fault, implying that the foreland was largely unaffected by Mesozoic rifting. No strata younger than Campanian are preserved south of the thrust front.

South of the North Pyrenean Frontal Thrust, Triassic evaporites (Keuper Group; unconstrained thickness) lie at the base of the Roquefeuil and Fougax block successions (Marty, 1976). Jurassic limestones and dolomites occur across the northern North Pyrenean Zone (Black Dolomite Group; 100 to 200 m; Figure 2). Berriasian to Barremian limestones are present in the Roquefeuil block (1,000 m, Mirande Group; Figure 3b) but absent in the Fougax and Nalzen blocks (Figures 4 and 5). These strata record littoral environments, with occasional lagoonal and distal platform deposits (Bilotte, Cosson, et al., 1988).

In the Metamorphic Internal Zone (Figure 2; Choukroune, 1974), protolith carbonates and siliciclastic strata are interpreted as Jurassic to Early Cretaceous in age (Golberg & Leyreloup, 1990; Lagabrielle et al., 2010), but their true age remains unclear owing to Albian to Cenomanian high-temperature, low-pressure metamorphism and strong internal deformation (Golberg & Leyreloup, 1990). Widespread breccias predominantly consist of clasts of marble and hornfels, but also rare clasts of basement rocks and mantle lithologies (de Saint Blanquat et al., 2016).

Syn-rift deep marine shales of the Black Flysch Group (~1,000 m; Aptian to lower Cenomanian) are in stratigraphic continuity with the Mirande Group limestones on the southern Fougax block (Figures 2 and 5), while on the northern side they rest unconformably on the Jurassic Black Dolomite Group (Bilotte, Cosson, et al., 1988). The term "flysch" is traditionally used in the name of the mid-Albian to lower Cenomanian "Black Flysch" Formation, despite its pre-orogenic origin (Debroas, 1990; Souquet et al., 1985). Here we apply the name "Black Flysch Group" to a wider age range due to very similar lithologies of Aptian to lower Albian age. Black Flysch shales transition northward into rudist platform limestones (Urgonian facies) of equivalent age (Figure 3b) and of variable thickness (maximum ~600 m; Bilotte, Cosson, et al., 1988). The Black Flysch Group thins westward where it is preserved in the Nalzen block north of the Saint-Barthélémy Massif (~600 m;

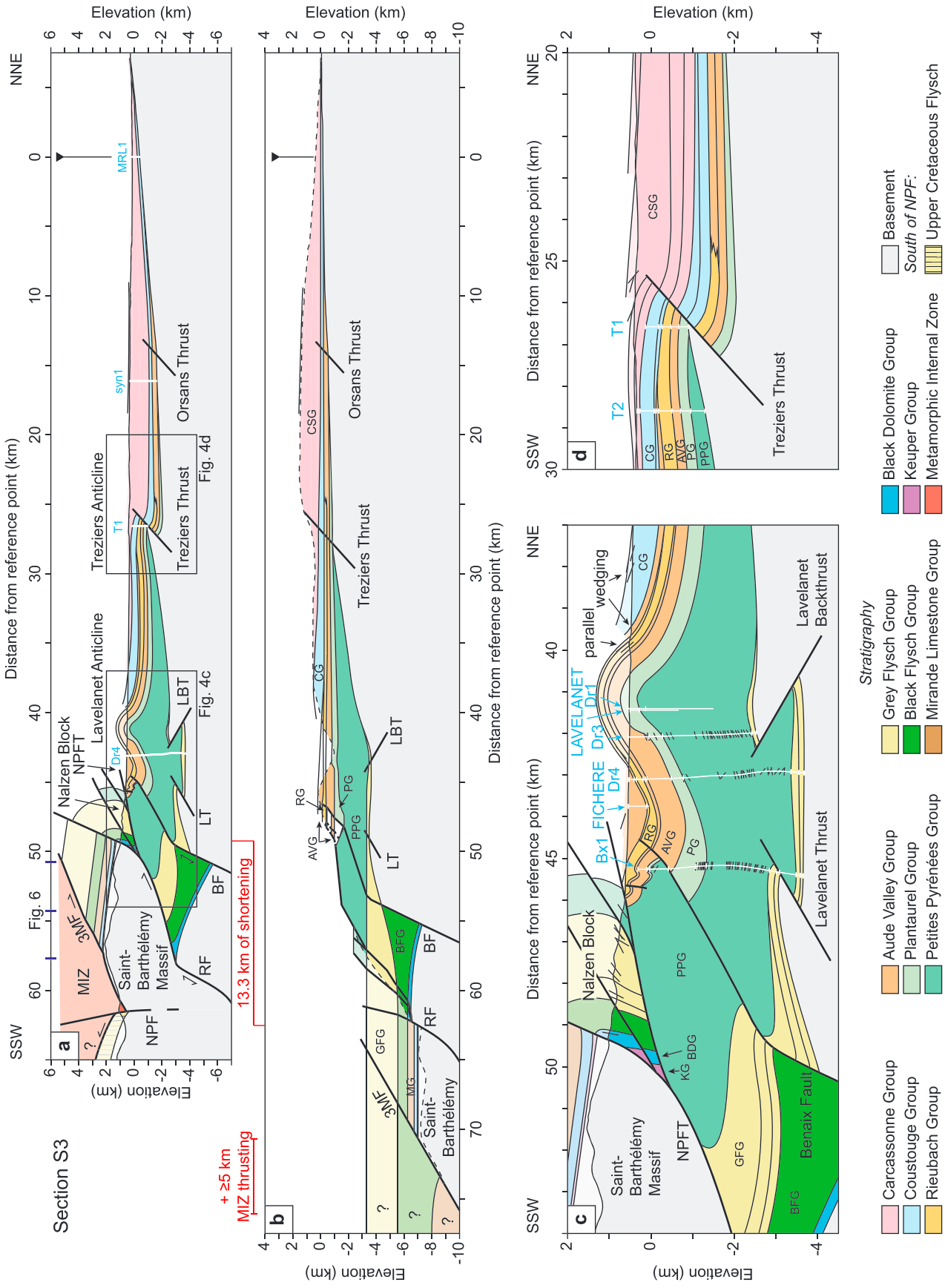

Figure 4. (a) Balanced and (b) restored cross section S3, located on Figures 1 and 2. (c, d) Details of the Lavelanet and Treziers Anticline located in Figure 4a. Semitransparent areas represent extrapolation above erosion level. White lines with blue letters indicate boreholes. MIZ, Metamorphic Internal Zone; NPF, North Pyrenean Fault; 3MF, 3M Fault; RF, Roquefeuil Fault; BF, Benaix Fault; NPFT, North Pyrenean Frontal Thrust; LT, Lavelanet Thrust; LBT, Lavelanet Backthrust. See Figure 5 for key to structural data. See text for details.

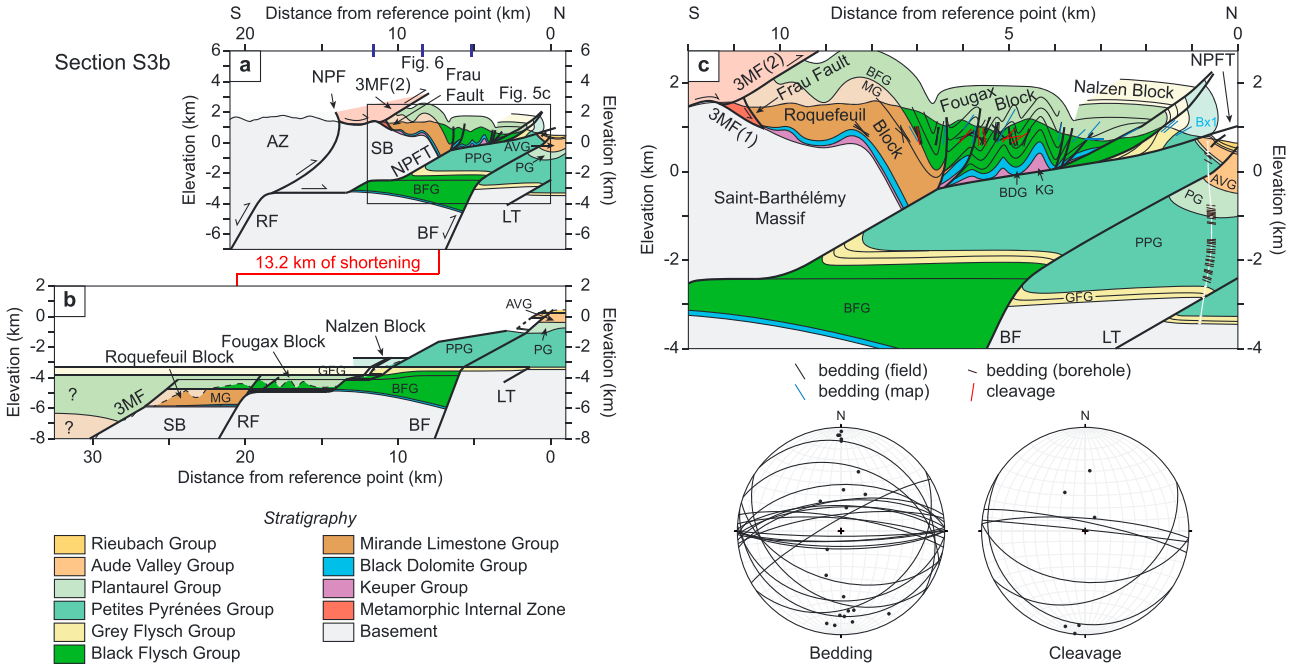

Figure 5. (a) Balanced and (b) restored cross section S3b, located on Figures 1 and 2. (c) Details of Figure 5a. Semitransparent areas represent extrapolation above erosion level. AZ, Axial Zone; SB, Saint-Barthélémy Massif; NPF, North Pyrenean Fault; 3MF, 3M Fault; 3MF(1), flat of 3M Fault; 3MF(2), hanging wall shortcut of 3M Fault; RF, Roquefeuil Fault; NPFT, North Pyrenean Frontal Thrust; BF, Benaix Fault; LT, Lavelanet Thrust. See text for details.

Figure 2), thus recording stratigraphic continuity between the Fougax and Nalzen blocks. There, these shales contain marine conglomerates with locally sourced basement clasts (Conglomérat de Freychenet; Bilotte, Cosson, et al., 1988).

The post-rift Grey Flysch Group succession (Cenomanian to Santonian) records a deepening upward trend from platform carbonates to deep-water marls (borehole Dr4; Figure 3b). South of the North Pyrenean Frontal Thrust, it is only preserved in the Nalzen block (Figure 2; 1,000 to 1,500 m). To the north it directly overlies a partially inverted half-graben and Variscan basement (Figure 5) and thins northward to pinch out north of the Lavelanet Anticline (Figure 4c). There, Santonian strata are either missing or indistinguishable from the overlying syn-orogenic sediments. Santonian sediments are unlikely to have been eroded completely, given the marine depositional environment. Therefore, we interpret this as local nondeposition, recording southward offlap of the upper Grey Flysch Group.

The Petites Pyrénées Group represents the early syn-orogenic succession (Lower to Middle Campanian; Figures 3b, 4, and 5). South of the North Pyrenean Frontal Thrust, the succession reaches a minimum thickness of ~500 m (Nalzen block) and records shallower and more sandy facies than further north. North of the Frontal Thrust, the group thins northward from between 1,500 to 2,500 m to pinch out in the Tréziers Anticline (Figures 3b and 4). Internal deformation is responsible for thickening of the Petites Pyrénées Group below the Lavelanet Anticline. The northern series records a shallowing upward trend from deep marine shales (with secondary siltstones and sandstones) representing delta progradation from east to west (Bilotte, 1985; Ricateau & Villemin, 1973). It is overlain by and laterally equivalent to the fluvio-deltaic Plantaurel Group (late Campanian to middle Maastrichtian) that was supplied from the east with rare marine incursions from the west (Bilotte, 1985; Bilotte, Cosson, et al., 1988). The Plantaurel Group thickens northward from 300 m to 1,300 m across the syn-depositionally inverted Benaix Fault and then gradually thins northward to 700 m in the Lavelanet Anticline, reaching 430 m in the Tréziers Anticline before pinching out around Orsans (Figures 3b and 4).

North of the North Pyrenean Frontal Thrust, red continental muds, sandstones, and intercalated conglomerates of the Aude Valley Group (Garumnian facies; middle Maastrichtian to Thanetian) unconformably overlie the Plantaurel (Lavelanet Anticline; Figure 2; Bilotte, Cosson, et al., 1988) and Petites Pyrénées Groups (near Benaix; Figure 2). The Maastrichtian conglomerates contain pebbles of Upper Cretaceous limestones

(Bilotte, Cosson, et al., 1988), recording exhumation and erosion in the hinterland. In borehole Dr4 locally developed Danian to Selandian lacustrine limestones and marls are only ~95 m thick (Table A3). A brief Thanetian marine incursion is recorded in the southern half of the basin by internal platform limestones of the Rieubach Group, which is the western equivalent of, and interfingers with, the continental Aude Valley Group (Ford et al., 2016). Growth strata only appear in the upper Thanetian portion of the succession (Figure 4c). Overall, the Aude Valley Group thins northward from 700 m south of the Lavelanet Anticline to pinch out just south of borehole MRL1 (Figures 3b and 4).

A more significant but brief marine incursion in the early Ypresian (Ilerdian) is recorded across the entire eastern foreland basin at the base of the Coustouge Group (Bilotte, Cosson, et al., 1988; Cavaillé et al., 1975b; Cavaillé, 1976a). This group then records a shallowing upward trend with marine marls and limestones passing up into mudstones and nummulitic sandstones (Bilotte, Cosson, et al., 1988; Tambareau et al., 1995). Thicknesses vary considerably due to syn-sedimentary deformation: from ~700 m immediately north of the Lavelanet Anticline to ~450 m in the Tréziers Anticline, ~500 m in the footwall of the Tréziers Thrust, to ~100 m at the northern limit of the preserved foreland basin (borehole MRL1). The northern pinchout is not preserved (Figure 1a). The Late Ypresian to Rupelian Carcassonne Group covers the entire foreland north of the Lavelanet Anticline, with the main depocentre in the footwall of the Tréziers Thrust (Figure 4). These sediments consist of mainly fluvial sandstones. Proximal conglomerates along the thrust front include clasts of crystalline basement, scapolite-bearing limestones, impure marble with garnets, and nonmetamorphic Mesozoic sediments, sourced from the south (Bilotte, Cosson, et al., 1988; Crochet, 1991).

4.2. North Pyrenean Structure

The structure of the eastern North Pyrenean Zone in the Saint-Barthélémy-Fougax area is here described along two restored cross sections (S3 and S3b; Figures 4 and 5). Restoration provides estimates of N-S shortening across the whole northern wedge of 13.3 km (S3) and 13.2 km (S3b), excluding emplacement of the Metamorphic Internal Zone (minimum ~5 km). This is lower than previous estimates of around 25–30 km that also excluded emplacement of the Metamorphic Internal Zone (Baby, 1988; Baby et al., 1988; Souquet & Peybernès, 1987). Most of this difference comes from a basement duplex proposed below the Saint-Barthélémy Massif that is not necessary to fit our data and thus is absent in our interpretation.

In the Aquitaine Basin, the sedimentary infill is gently deformed by the basement-rooted Tréziers and Orsans Thrusts (Figures 4a and 4d). Both structures are the western terminations of thrusts accommodating large anticlinal basement uplifts in the eastern foreland: the Mouthoumet (Bilotte, Cosson, et al., 1988; Cavaillé, 1976a; Crochet et al., 1989) and Alaric thrusts (Christophoul et al., 2003; Ellenberger et al., 1987).

The WNW-ESE trending Lavelanet Anticline is the most prominent surface feature of the sub Pyrenean Zone (Figure 2). Boreholes (Dr3, Dr4) reveal a 1,150 m difference in basement depth below the southern flank (Figure 4c), interpreted here as due to a south-verging thrust (Lavelanet Backthrust; Baby, 1988). Repetition of stratigraphy in borehole Bx1 implies the existence of two other blind, north-verging thrusts (Benaix Fault and Lavelanet Thrust; Figure 4c). The Benaix Fault is a partially inverted normal fault delimiting a Lower Cretaceous rift basin that is equivalent to the Camarade basin to the west (Ford et al., 2016).

The North Pyrenean Frontal Thrust marks an abrupt southward increase in deformation intensity (Figures 4 and 5). The fault is here interpreted as an inverted normal fault with the deformed Nalzen-Fougax basins in its hanging wall. The Nalzen succession (S3; Figure 4) forms the vertical to overturned limb of a major north verging anticline cored by the Saint-Barthélémy basement (Figure 4c). We interpret this structure as a basement-cored forced fold, similar to Laramide structures with a larger fault offset (e.g., Mitra & Mount, 1998). Several hanging wall splays of the main North Pyrenean Frontal Thrust cut the Nalzen block. This basement-cored forced fold transitions into a recumbent fold with no basement ~5 km to the east, on section S3b (Figure 5), where the Fougax block is thrust over the overturned frontal limb.

In the Fougax block, Black Dolomite and Black Flysch strata are intensely folded and cleaved (Figure 5; Marty, 1976). The E-W trending, tight, upright folds show a short wavelength of ~750 to 850 m and relatively low amplitudes of ~500 to 600 m. Using the methods described in Bulnes and Poblet (1999), we use the fold geometry to infer a depth to décollement of approximately 1 to 1.5 km. This suggests that the Fougax and Nalzen successions were detached from their basement (probably along Keuper evaporites; Marty, 1976), folded and thrust northward above the North Pyrenean Frontal Thrust. Baby (1988) proposes that the Nalzen basin is

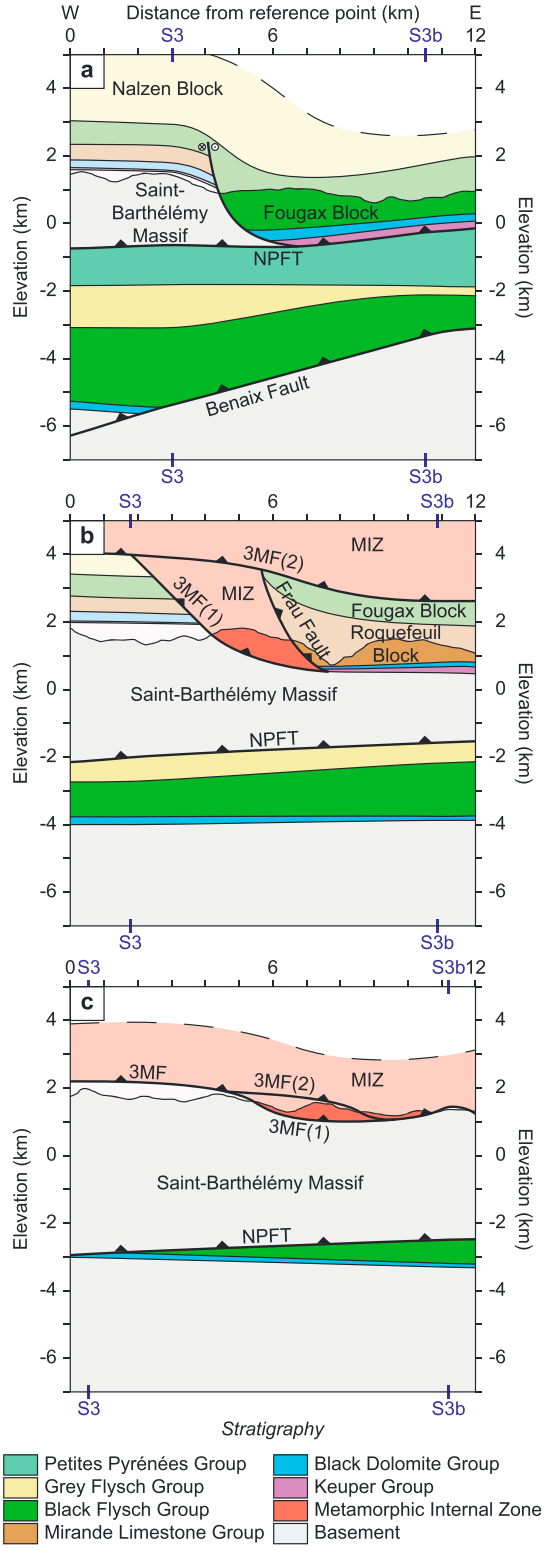

Figure 6. Lateral sections illustrating the three-dimensional structure of the Frau area. (a, b, c) Northern, middle, and southern sections in Figure 2, respectively. Semitransparent areas represent extrapolation above erosion level. MIZ, Metamorphic Internal Zone; NPFT, North Pyrenean Frontal Thrust; 3MF, 3M Fault; 3MF(1), flat of 3M Fault; 3MF(2), hanging wall shortcut of 3M Fault; BF, Benaix Fault.

immediately underlain by a basement high, implying the same for the Fougax Basin. Given the difference between the estimated depth of the Fougax decollement and the observed depth of basement in boreholes further north, this model requires a throw of 3 km on an unknown north vergent thrust. The two blind thrusts observed in borehole Bx1 do not accommodate sufficient shortening to produce the required displacement. In addition, our interpretation of the Nalzen Block means it was cut from the footwall of the Roquefeuil Fault; thus, Black Flysch Group strata should also be present at depth in the footwall of the North Pyrenean Frontal Thrust. We therefore extrapolated the foreland basin succession in borehole Bx1 southward (~4 km) to underlie the allochthonous Fougax and Nalzen blocks and overlie a partially inverted rift basin that is equivalent to the Camarade basin to the west (Figures 4c and 5c; Ford et al., 2016).

Folds of the Roquefeuil block have a wavelength of ~1.5 to ~2.5 km (Figures 2 and 5c). The southward twofold increase in fold wavelength is abrupt and is interpreted to indicate a change in depth to the basal thrust. Because Mirande Group limestones are clearly absent below the northern Fougax block, we propose that they are limited to the north by a blind inverted extensional basin margin fault (Roquefeuil Fault; Figure 5b) sealed by the Black Flysch Group.

The Saint-Barthélémy Massif is a large block of Paleozoic metasediments and crystalline basement (de Saint Blanquat, Lardeaux, & Brunel, 1990). The top of basement drops eastward to a deeper level across an east-dipping lateral ramp to lie below the Metamorphic Internal Zone (Souquet & Peybernès, 1987) and the Roquefeuil block, as evidenced by the small tectonic windows around Camurac (Figures 2 and 6). South of Montségur, a syncline of the Fougax block plunges steeply eastward (Figure 2; Bilotte, Cosson, et al., 1988) across the same lateral ramp. This lateral ramp is interpreted here as a reactivated Cretaceous extensional structure that may also be responsible for the westward thinning of the Lower Cretaceous sedimentary cover of the Saint-Barthélémy Massif. The massif has previously been interpreted as an allochthonous unit that originally formed a basement high south of the Nalzen block (Baby, 1988; Baby et al., 1988; Souquet & Peybernès, 1987). Apatite fission track data from the adjacent Arize Massif imply that the massifs were buried before the Eocene (Vacherat et al., 2016). Assuming a standard geothermal gradient of 30°C/km and closure temperature of 100–120°C (Reiners, 2005), the massifs were buried to at least 3–4 km by Mesozoic sedimentary cover (Black Flysch Group, Grey Flysch Group, and possibly Petites Pyrénées Group). This is consistent with our restoration that places the massif below the ~4 km thick Nalzen block, which requires less shortening than earlier restorations (Baby, 1988; Baby et al., 1988).

The amount of Pyrenean shortening accommodated in the Metamorphic Internal Zone and its displacement along the 3M Fault (Figures 2, 4, 5, and 6; Marty, 1976) cannot be quantified due to intense metamorphism and internal deformation (mainly brecciation). The 3M Fault curves around the SE corner of the Saint-Barthélémy Massif and across the lateral ramp from a steep north-verging thrust along the massif's southern boundary (Figures 4 and 5) to a subhorizontal orientation to the east in the Camurac area (3MF(1); Figures 2 and 6b; de Saint Blanquat et al., 2016). The subhorizontal 3M Fault terminates northward

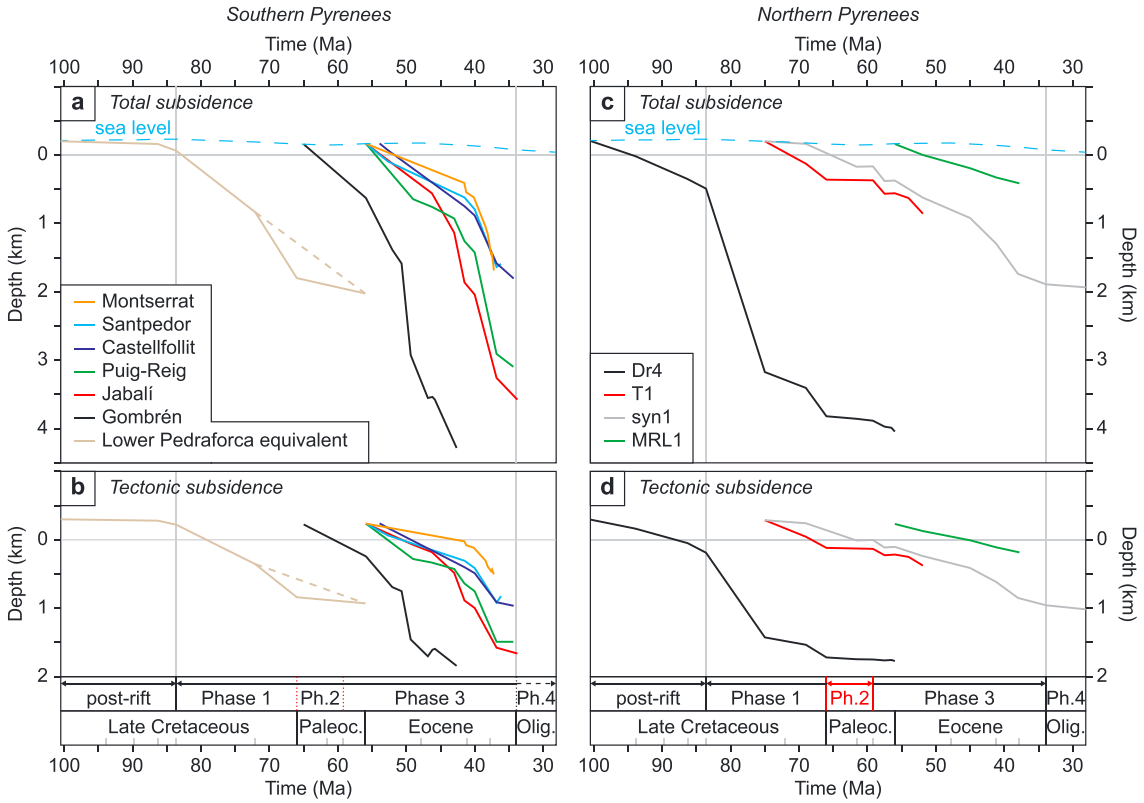

Figure 7. Total subsidence and tectonic subsidence curves for the (a, b) southern and (b, c) northern Pyrenees. All depths are relative to present-day sea level. (a, b) Due to uncertain dating of strata, the solid line of the lower Pedraforca equivalent shows Maastrichtian and Paleocene subsidence as maximum and minimum rates, respectively. The dashed line shows an average subsidence rate. Other south Pyrenean subsidence data from Vergés et al. (1998). Detailed supporting data are available as Tables A2, A3, and A4 in the supporting information.

against a north dipping tectonic boundary (Frau Fault) with the Roquefeuil succession in its hanging wall (Figures 5c and 6b). The Frau Fault branches onto the 3M Fault to the west and is cut by a north-vergent hanging wall splay of the 3M Fault (3MF(2) to the east; Figures 2 and 6).

The North Pyrenean Fault juxtaposes the Metamorphic Internal Zone against the Axial Zone. Following interpretations of the ECORS deep seismic line (e.g., Muñoz, 1992; Figure 1b), the North Pyrenean Fault terminates downward against the North Pyrenean Frontal Thrust, which carries the Axial Zone on top of European basement (Figures 4a and 5a).

4.3. Syn-Orogenic Subsidence of the North Pyrenean Foreland

The unrifted Pyrenean foreland records gentle post-rift subsidence only in its proximal zone (<0.03 mm/yr in Dr4; Figures 7c and 7d; Table A3). Syn-orogenic subsidence curves display a coherent trend across the foreland with two clear periods of subsidence separated by a quiescent phase (Figures 7c and 7d). Overall syn-orogenic tectonic subsidence is characterized by very low rates with only 0.06 mm/yr on average for Dr4, which records the fastest subsidence. A sharp increase in subsidence rate at ~84 Ma marks the onset of convergence, reaching a maximum of 0.14 mm/yr during the early Campanian. Subsidence slowed down after 75 Ma to 0.02 mm/yr and 0.04 mm/yr in boreholes Dr4 and T1, respectively. Little or no subsidence was recorded throughout the foreland from ~66 to ~59 Ma (quiescent phase). The subsidence shown in the synthetic borehole syn1 during the first half of this phase is probably an artifact due to poor age control. Renewed subsidence started in the more distal basin during the Thanetian (~59 Ma, Figures 7c and 7d) and is characterized by lower tectonic subsidence rates than during the Late Cretaceous (0.03 mm/yr and 0.09 mm/yr on average, respectively). These long-term averages are based on tectonic subsidence of 1,530 m in 18 Myr (borehole Dr4) and 244 m in 7.3 Myr (borehole T1). Borehole syn1 shows a gradual slowing of subsidence toward the end of the Eocene.

4.4. Evolution of the North Pyrenean Wedge and Foreland

The model presented here for the evolution of the North Pyrenean wedge and foreland in the Saint-Barthélémy-Fougax area is based on the restorations of the cross sections S3 and S3b (Figures 4 and 5), foreland basin subsidence history, and the construction of three lateral cross sections linking the two present-day cross sections (Figure 6). The age boundaries of the evolutionary phases correspond to rounded boundaries of international chronostratigraphic ages due to limitations in the available stratigraphic dating (Bilotte, Cosson, et al., 1988; Cavaillé, 1976b).

4.4.1. Early Cretaceous Rift and Late Cretaceous Post-Rift Phases

The mildly metamorphic (up to 200°C; Gouache, 2017) North Pyrenean Zone represents the European margin of the Apto-Cenomanian hyperextended rift system. Early Cretaceous extension was focused mainly further south, where thinning of the crust exhumed mantle between the Iberian and European plates. The Metamorphic Internal Zone is thought to have overlain the zone of exhumed mantle (Ford et al., 2016; Lagabrielle et al., 2010; Mouthereau et al., 2014; Tugend et al., 2015). The Roquefeuil and Benaix Faults (Figures 5b and 6b) represent the proximal northern margin of the rift system and accommodated ~1.5 km of N-S extension. The Roquefeuil Fault was active from Berriasian to Barremian. In the Aptian, the rift deepened and its margin migrated north to the Benaix Fault whose footwall was eroded to basement. A N-S lateral ramp delimited the Saint-Barthélémy high to the west, although the Mirande Group may still have covered it. Deep marine strata (Black Flysch Group) were deposited from the Aptian to Cenomanian, thinning westward across the lateral ramp.

The post-rift basin progressively deepened as its margin migrated northward, onlapping unrifted basement, from middle Cenomanian to approximately Middle Turonian times, followed by progressive offlap until end Santonian (Figure 8d). Following Ford et al. (2016) and Vacherat et al. (2016), we propose that the post-rift Grey Flysch extended south to cover the whole rift zone.

4.4.2. First Orogenic Phase: 84–66 Ma, Early Inversion

During early convergence, the Metamorphic Internal Zone was emplaced northward along the 3M Fault. Gentle inversion affected inherited normal faults of the European margin and began folding Mesozoic basin successions (Nalzen, Fougax). Estimated shortening rates were 0.3–0.6 mm/yr, the latter value including a minimum of shortening related to emplacement of the Metamorphic Internal Zone. Early inversion of the margin is not recorded by low temperature thermochronological data from the adjacent Arize Massif (Fitzgerald et al., 1999; Vacherat et al., 2016), suggesting that early basement exhumation was limited. A deep marine flexural basin was supplied with sediment mainly from the east (Bilotte, 1985). Tectonic subsidence was relatively rapid though still only 0.09 mm/yr close to the thrust front (Table 1). We relate this early subsidence to emplacement of the Metamorphic Internal Zone and early inversion and crustal thickening along the European margin. Campanian strata preserved in the Nalzen block indicate that the foreland basin continued south of the thrust front, implying that the early orogenic edifice had low topographic relief and remained largely submarine. Shallower water facies in the Nalzen block suggest a syn-sedimentary uplift along the North Pyrenean Frontal Thrust within the subsiding basin. The foreland basin records a deepening and then shallowing upward trend, ending in fluvial conditions across the entire foreland. Aude Valley Group strata contain clasts of Upper Cretaceous limestones that were either sourced from the east, the south, or from local uplifts (Bilotte, Cosson, et al., 1988).

4.4.3. Second Phase: 66–59 Ma, Northern Quiescence

During the early Paleocene, no fault activity was recorded. Tectonic subsidence slowed to near zero in the foreland with deposition of only a thin unit of fine-grained continental deposits. This quiescence is also documented further west (Ford et al., 2016; Rougier et al., 2016), suggesting it was a widespread phase in the northern Pyrenees.

4.4.4. Third Phase: 59–34 Ma, Slow Northern Activity

Tectonic activity returned in the Thanetian with distributed thick-skinned shortening across the North Pyrenean wedge. The shortening rate was lower than in the Late Cretaceous, at 0.3 mm/yr on average (Table 1). A slight acceleration in foreland basin subsidence was associated with a minor marine incursion across the proximal foreland (Rieubach Group; Figure 3b). Continental facies were then deposited across the whole foreland. More widespread deformation returned in the early Ypresian (~56 Ma), with activity on the Tréziers Thrust and Lavelanet Anticline. A basin-wide marine incursion can be related to a eustatic sea level rise (Coustouge Group; Christophoul et al., 2003). Widespread continental sedimentation

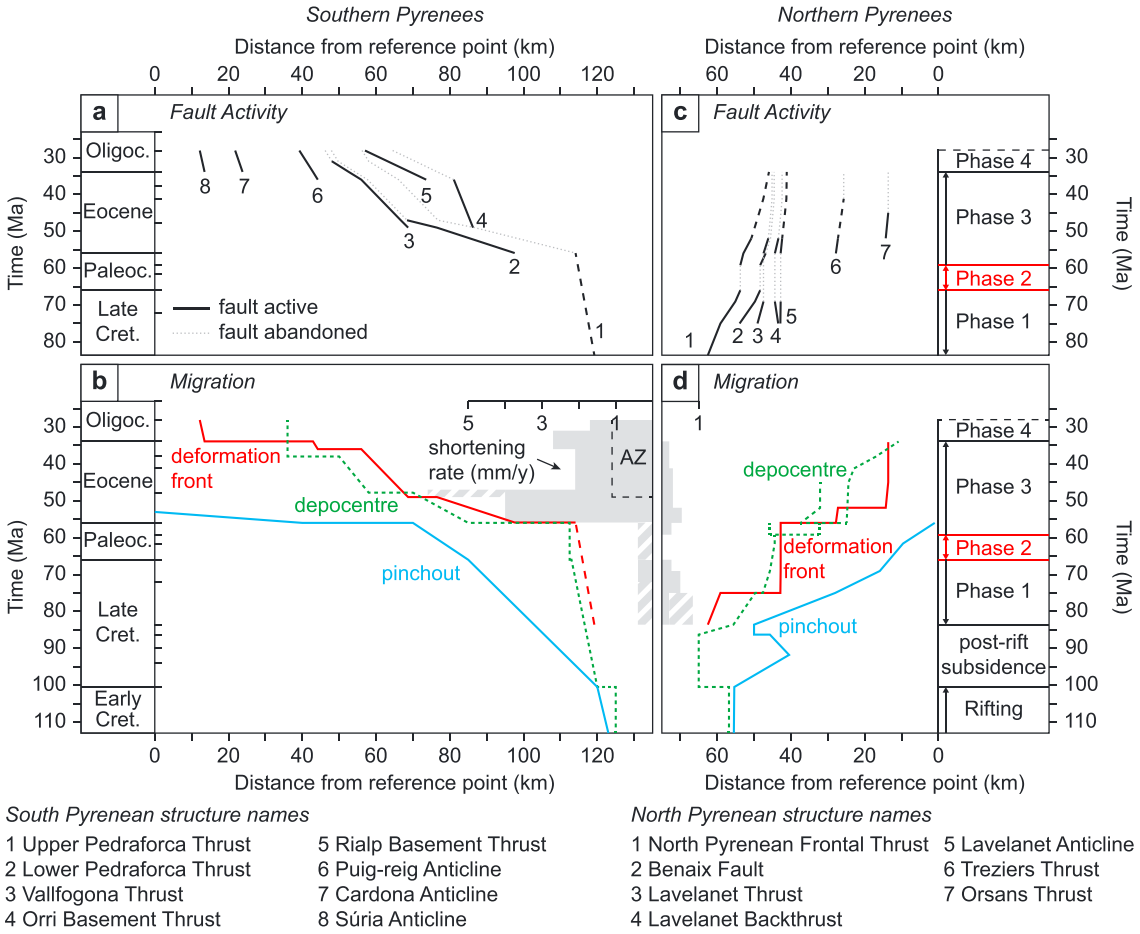

Figure 8. (a, c) Reconstruction of the distribution of shortening through time in the southern Pyrenees (J3 section; Figure 9) from Vergés (1993) and northern Pyrenees (S3 section; Figures 4 and 5). Each line represents either the horizontal position of the leading edge of a principal fault or the position of the hinge zone at the surface of a major anticline. Displacement and fault length are assumed to increase linearly for each fault. For emergent faults, we assumed the fault reached maximum length during deposition of youngest cut strata. Fault timings for the southern Pyrenees from fault-strata relationships (Costa et al., 2010; Carrigan et al., 2016; Ford et al., 1997; Ramos et al., 2002; Vergés & Martinez, 1988; Vergés et al., 1995, 1998, 2002). (b, d) Horizontal position of the deformation front, the main depocenter(s), and foreland pinchout of the basin as a function of time in the southern and northern Pyrenees, respectively. The deformation front tracks the location of the most frontal structure through time. Depocenters were measured from balanced cross sections. Pinchout locations were determined from borehole and seismic data. Shortening rates through time are shown by gray bars, derived from the fault activity in Figures 8a and 8c. Shortening rates for the south include internal shortening in the Axial Zone (AZ). Dashed bars have a high uncertainty for the early convergence.

(Carcassonne Group) was reestablished at the end of the Ypresian and continued until at least Rupelian times (Figure 3b). Post-Thanetian activity of the North Pyrenean Frontal Thrust until at least lower Ypresian is recorded north of the Nalzen block. Uplift and erosion of the Metamorphic Internal Zone, Saint-Barthélémy Massif, and/or the Axial Zone are recorded by pebbles of metamorphosed limestone and crystalline basement in Carcassonne Group conglomerates (Crochet, 1991). Subsidence was slower during this phase at ~0.03 mm/yr near the basin depocentre. The deformation front migrated northward, progressively activating basement-involved thrusts in the foreland (Tréziers and Orsans thrusts). The basin depocentre followed and usually lay behind the deformation front (Figure 8d). The youngest evidence for deformation in the North Pyrenean foreland is the slight folding of the upper Carcassonne Group above the Tréziers Thrust, dated as approximately Priabonian (Figure 4d).

4.4.5. Fourth Phase: 34–28 Ma, Final Abandonment

Due to Miocene uplift of the Massif Central north of this part of the Pyrenean foreland basin, the Early Oligocene record is incomplete. We have no record of any fault activity during this phase, and it appears that the Tréziers and Orsans thrusts were abandoned at the end of the preceding phase, as they are sealed by the upper Carcassonne Group.

Table 1
Tectonic Subsidence Rates and Shortening Rates in the Eastern Pyrenees[a]

Orogenic phase	Tectonic subsidence rate (mm/yr)		Shortening rate (mm/yr)	
	South[b]	North[c]	South[b]	North[c]
84-66 Ma	0.06	0.09	0.4	0.6
66–59 Ma	0.05	0.00	0.4	0
59–34 Ma	0.12	0.03	2.7	0.3
34–28 Ma	—	0.01	2.2	0

[a]All rates were averaged over their respective phases. [b]Combines the Axial Zone, South Pyrenean Zone, and Ebro foreland basin. [c]Combines the North Pyrenean Zone, sub Pyrenean Zone, and Aquitaine foreland basin.

5. South Pyrenean Foreland

We performed a similar analysis of the South Pyrenean foreland along transect J3 (Figure 9; Vergés, 1993). This 120 km long balanced cross section stretches from the Axial Zone in the north to the Catalan Coastal Ranges in the south, traversing the eastern South Pyrenean Zone and Ebro Foreland Basin (Figure 1). The section was constrained by borehole data, surface geology, and seismic lines. A detailed description of this area can be found in Vergés et al. (1995, 1998, 2002), and only a summary is given here. Total shortening in the South Pyrenean foreland is 69.2 km, not accounting for internal deformation in the Axial Zone (~23 km; Vergés et al., 1995) and Catalan Coastal Ranges (Figure 9).

5.1. Stratigraphy of the South Pyrenean Foreland

Upper Triassic Keuper evaporites serve as a basal detachment for the Upper and Lower Pedraforca thrust sheets in the South Pyrenean Zone but is absent further south below the Ebro Basin, except close to the Catalan Coastal Ranges (Figure 9). A thin Liassic limestone and dolomite succession is only found in the Pedraforca thrust sheets. Cretaceous strata are mostly found in the Pedraforca thrust sheets and thin southward over a distance of 10 km (Figure 9b; Vergés, 1993). The Upper Pedraforca thrust sheet, which restores to the most northerly position, mainly consists of a ~1,500 m thick inverted Lower Cretaceous extensional basin. The Lower Pedraforca thrust sheet contains ~1,700 m of post-rift and syn-orogenic Upper Cretaceous conglomerates, marls, and limestones, capped by ~700 m of Maastrichtian to Paleocene red beds (Garumnian facies) of the Tremp Formation (Figure 3a; Vergés et al., 1994; Vergés & Martinez, 1988).

A regional unconformity marks the base of Eocene marine sedimentation in the South Pyrenean foreland (Pujalte et al., 1994; Serra-Kiel et al., 1994; Vergés et al., 1998). These marine sediments overlie the Tremp Formation in the north and onlap basement further south. They record four transgressive-regressive cycles from Ypresian to Bartonian (Martinez et al., 1989; Puigdefàbregas & Souquet, 1986; Vergés et al., 1998). Within each cycle, terrigenous clastic deposits were deposited in front of the advancing South Pyrenean Thrust Front (Corones, Bellmunt, and Milany Formations; Figure 3a). These depositional units grade southward into moderate to deep-water marine carbonates and calcareous mudstones (Sagnari, Armáncies, Campdevánol, and Banyoles Formations; Figure 3a) that, in turn, grade into shallow marine platform carbonates (Cadí, Penya and Tavertet Formations; Figure 3a) toward the southernmost border of the foreland basin. During the fourth cycle, the basin was characterized by prodelta offshore marls (Igualada Formation; Figure 3a) bounded by northward prograding fan-delta deposits sourced from the uplifting Catalan Coastal Ranges in the south (Montserrat Formation; Figure 3a) and southward prograding Milany Formation in the north. At the end of cycles 2 and 4, thick evaporitic units are deposited in the central marine basin, the marine Beuda and transitional Cardona Formations, respectively (Figure 3a). In the footwall of the Vallfogona thrust, the Beuda evaporites reach 2,000 m thickness, including a 200 m thick package of salt (Martinez et al., 1989). The Ebro foreland basin became fully continental during the deposition of the uppermost part of the Cardona evaporitic Formation at ~36 Ma (middle Priabonian; Costa et al., 2010). Widespread nonmarine deposition was then established until the latest Oligocene consisting of the alluvial and fluvial Solsona Formation and equivalent lacustrine deposits in the center of the foreland basin (Figure 3a; García-Castellanos et al., 2003; García-Castellanos & Larrasoaña, 2015; Meigs et al., 1996; Valero et al., 2014).

5.2. Structure of the South Pyrenean Foreland

The South Pyrenean foreland fold-and-thrust belt, here called the South Pyrenean Zone, lies between the antiformal Axial Zone to the north and the mildly deformed Ebro foreland basin to the south (Figure 1b; Vergés et al., 2002). In the Eastern Pyrenees, three stacked thrust sheets compose the South Pyrenean Zone, namely from top (oldest) to bottom (youngest), the Upper Pedraforca, the Lower Pedraforca, and the Cadí thrust sheets (Figure 9). The Upper Pedraforca and Lower Pedraforca thrust sheets are mostly constituted by Jurassic to Paleocene units detached above the Keuper evaporites. The Vallfogona thrust transports the Cadí thrust sheet with the Upper and Lower Pedraforca thrust sheets in its hanging wall.

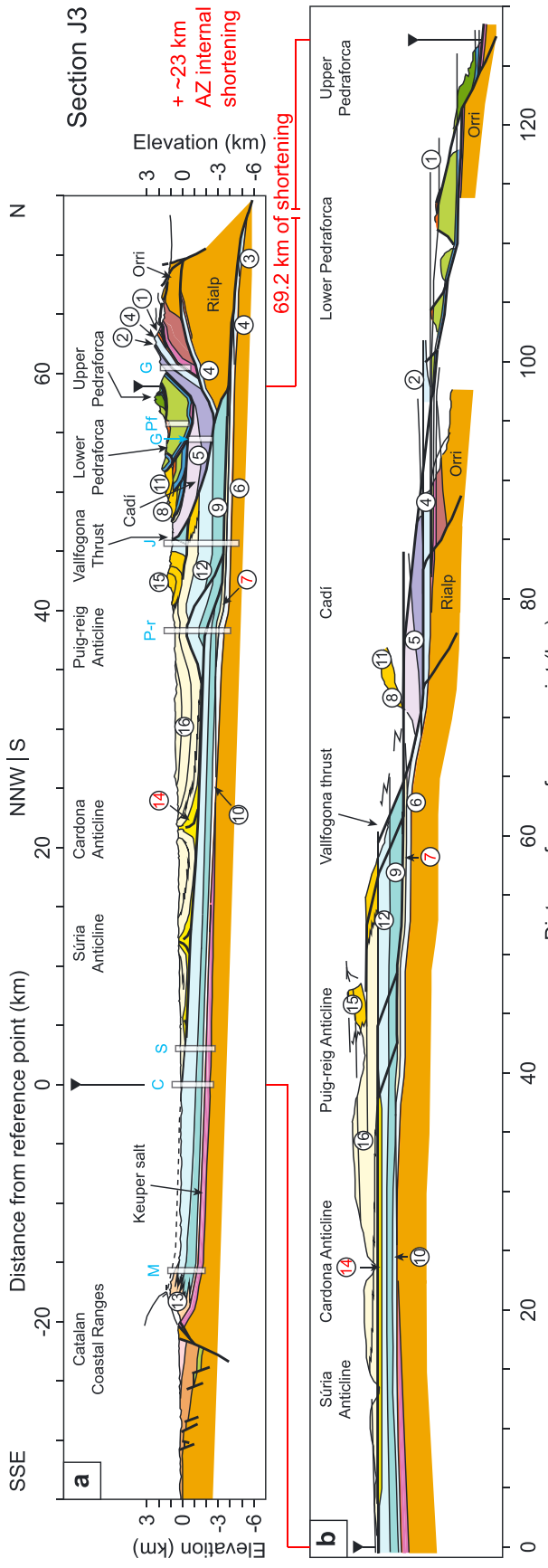

Figure 9. Balanced and restored cross section J3 in the south Pyrenean pro-foreland. Simplified after Vergés (1993). Boreholes and stratigraphic sections used for subsidence calculations are indicated as semitransparent white boxes with blue letters. M, Montserrat; C, Castellfollit; S, Santpedor; P-r, Puig-reig; J, Jabalí; G, Gombrèn (split in two); Pf, Pedraforca. Formation names are indicated by numbers in circles as in Figure 3a.

Following Vergés (1993) and Vergés et al. (1995, 2002), the Pedraforca thrust sheets root below the Nogueres basement thrust sheet of the Axial Zone, whereas the Vallfogona thrust links back to the Orri basement thrust (Figure 1b). Laumonier (2015) alternatively suggests that the Pedraforca thrust sheets may root north of the North Pyrenean Fault, forming part of a "supra-axial unit." This model depends on the interpretation of the eastern Axial Zone as a single block. The kinematics of the supra-axial unit proposed by Laumonier (2015) implicitly require coeval closure of the exhumed mantle domain and emplacement of the Lower Pedraforca thrust sheet, which is inconsistent with our data (see sections 5.4.2 and 6.2). Alternatively, southward emplacement of the Pedraforca thrust sheets could be entirely gravitational, similar to the gravitational collapse of the cover into the Pyrenean basin during rifting (e.g., Saura et al., 2016). This would eliminate the need to root the Pedraforca thrust sheets into basement thrusts, although we have chosen not to use this model.

The Puig-reig anticline within the Ebro foreland basin is the surface expression of a thrust ramp that steps up from the Beuda evaporite horizon to the Cardona salt horizon (Figure 9). This thrust links back into the Rialp basal thrust in the Axial Zone. Further south, the Cardona and Súria anticlines are detached and thrust along the Cardona evaporite horizon (e.g., Vergés et al., 1992). The southern margin of the Ebro basin was the result of the thick-skinned inversion of the Tethyan Mesozoic basin of the Catalan Coastal Ranges from Lutetian to Chattian (Anadón, 1986; Gómez-Paccard et al., 2012; López-Blanco et al., 2000). The southern and eastern borders of the Ebro foreland basin were regionally uplifted during the Cenozoic extensional phase that opened the Western Mediterranean, thus tilting the entire southern foreland (e.g., Lewis et al., 2000).

5.3. Subsidence of the South Pyrenean Foreland

The four boreholes and two stratigraphic sections along section J3, analyzed by Vergés et al. (1998), record the main Eocene basin history (Figures 7a, 7b, and 9; Table A4). Of those, only the Gombrèn stratigraphic section records Paleocene subsidence. To represent the Late Cretaceous and Paleocene subsidence record for the northernmost part of the foreland basin, a new subsidence curve was constructed for the Lower Pedraforca thrust sheet, based on data from Vergés et al. (1994). Due to uncertain dating of strata, Maastrichtian and Paleocene subsidence are shown as maximum and minimum rates, respectively (Figures 7a and 7b). If these are assumed to represent true tectonic subsidence, the Lower Pedraforca thrust sheet appears to record very slow subsidence during the Paleocene ($<$0.01 mm/yr; Figure 7b; Table A4). However, the Gombrèn stratigraphic section, now located in the Cadí thrust sheet, records slightly faster tectonic subsidence in the Paleocene (0.05 mm/yr; Figure 7b; Table A4).

Subsidence accelerates in the Eocene, forming the classic convex-up subsidence pattern expected for pro-foreland basins (Sinclair & Naylor, 2012). Ypresian tectonic subsidence was high in the north of the Ebro foreland basin (Gombrèn section; 0.53 mm/yr around 50 Ma; Table A4), while rates were much lower to the south (0.03 to 0.07 mm/yr; Table A4). The onset of subsidence acceleration ($>$0.1 mm/yr) migrated south at a rate of about 10 mm/yr between 50.7 Ma and 40 Ma (Vergés et al., 1998). This outward migration is also typical of pro-foreland basins (Sinclair & Naylor, 2012). Increases in tectonic subsidence can be correlated with tectonic activity in the Axial Zone and South Pyrenean Zone (Figure 8a). For example, at 43 Ma, tectonic subsidence of the Jabalí and Puig-reig boreholes increased to 0.26 and 0.14 mm/yr, respectively, in response to loading by the Orri basement thrust sheet and emplacement of the Cadí thrust sheet (Vergés et al., 1998). Tectonic subsidence in the south (Montserrat section) sees a brief acceleration to 0.21 mm/yr at 41.5 Ma that can be correlated to activity of the Catalan Coastal Ranges (Vergés et al., 1998). After ~36 Ma, tectonic subsidence slowed down throughout the southern foreland basin (Figures 7a and 7b; Gómez-Paccard et al., 2012).

5.4. Evolution of the South Pyrenean Foreland

The summary of South Pyrenean foreland evolution given here is based on a compilation of subsidence and stratigraphic data and a restored cross section (Vergés, 1993). The boundaries of each evolutionary phase were chosen to reflect significant changes in the whole orogenic system and therefore do not necessarily correspond perfectly to distinct changes in the South Pyrenean foreland itself.

5.4.1. First and Second Phases: 84–59 Ma, Rift Inversion

The timing of the onset of shortening in the southern Pyrenees cannot be distinguished in the preserved subsidence signal and is not clear from the rest of our data. Growth strata related to the Boixols thrust,

carrying the western equivalent of the Upper Pedraforca thrust sheet, place the onset of shortening around ~72 Ma (Bond & McClay, 1995; Puigdefàbregas & Souquet, 1986). However, many authors place the onset of shortening in the southern Pyrenees at Late Santonian, or ~84 Ma (Ardèvol et al., 2000; McClay et al., 2004; Saura et al., 2016). In the Western Pyrenees, Teixell (1996) also places the onset of convergence at Late Santonian. A Late Cretaceous flexural basin is preserved in the Lower Pedraforca thrust sheet (Figures 7a, 7b, and 9b). We interpret this subsidence as a response to early inversion of the distal Iberian margin, during closure of the exhumed mantle domain. The Tremp Formation of latest Maastrichtian to upper Paleocene age seals the Upper Pedraforca thrust sheet (Vergés et al., 1995; Vergés & Martinez, 1988); however, tectonic subsidence appears to have continued very slowly throughout the Paleocene (Figure 7b; Table 1). Therefore, while we cannot rule out a Paleocene quiescence in the southern Pyrenees, sparse data appear to indicate slow shortening during the Paleocene. The first and second orogenic phases were characterized by the inversion of rift structures. Although poorly constrained, we estimate that ~10 km of shortening were accommodated between ~84 and ~56 Ma, yielding a rate of 0.4 mm/yr during the Late Cretaceous and Paleocene (Figure 8b; Table 1).

5.4.2. Third Phase: 59–34 Ma, Major Convergence

During early Eocene, shortening in the South Pyrenean foreland reached a maximum rate of 4.0 mm/yr (Figure 8b). South of the rapidly advancing thrust front, this was accompanied by an increase in tectonic subsidence (0.53 mm/yr maximum, Gombrèn; Figure 7b; Table A4), resulting in a deep marine basin (Figure 3a). Meanwhile, further south, tectonic subsidence rates and sediment supply were much lower (around 0.04 mm/yr), allowing the growth of carbonate platforms. Emplacement of the Lower Pedraforca thrust sheet occurred during early Eocene until ~47 Ma, as shown by syn-orogenic strata (Burbank, Puigdefàbregas, et al., 1992; Solé Sugrañes & Clavell, 1973; Vergés & Martinez, 1988).

Shortening slowed down significantly after the end of the Ypresian to 1.0 mm/yr (Figure 8b). A new basement thrust sheet (Orri) became active, as constrained by the Vallfogona thrust, marking the start of true thick-skinned frontal accretion (Figure 8a). Crustal thickening and exhumation in the Axial Zone started at ~50 Ma, recorded by low-temperature thermochronology data (Fitzgerald et al., 1999; Metcalf et al., 2009; Rahl et al., 2011; Sinclair et al., 2005; Whitchurch et al., 2011). Axial Zone deformation accommodated an average of 1.1 mm/yr of extra shortening until the end of convergence (~23 km since 50 Ma; Figure 8b; Vergés et al., 1995). This was accompanied by an increase in tectonic subsidence rates throughout the foreland basin to around 0.10 mm/yr (Figure 7b). The Gombrèn subsidence record in the proximal foreland shows a much lower rate starting in the late Ypresian, owing to deformation ahead of a propagating Vallfogona thrust, which reached the surface in the mid-Lutetian (Ramos et al., 2002; Vergés et al., 1998). Widespread growth strata within the Berga conglomerates (Figures 3 and 9) constrain the latest activity of the Vallfogona thrust to at least ~31 Ma (Figure 8a; Carrigan et al., 2016; Ford et al., 1997; Vergés et al., 1998). Most of the foreland basin remained marine to brackish, but sedimentation along the thrust front was continental from Lutetian onward (Figure 3a). The Cardona salt horizon was deposited around 36 Ma as a result of the isolation from the Atlantic Ocean after uplift of the Western Pyrenees (Burbank, Puigdefàbregas, et al., 1992; Costa et al., 2010; Vergés & Burbank, 1996). Growth strata on the flanks of the Puig-reig anticline date the onset of folding to around the same time (Vergés et al., 2002). This was related to the Rialp basement thrust and increased the shortening rate to 1.6 mm/yr (Figure 8b).

5.4.3. Fourth Phase: 34–28 Ma, Final Deformation

During this final phase, the shortening rate in the foreland decreased to 0.6 mm/yr (Figure 8b). Most shortening in the foreland was accommodated by detachment folding above the Cardona evaporites and the final activity of the Vallfogona thrust (Carrigan et al., 2016; Vergés et al., 1992). The deformation front thus rapidly migrated to the south along the Cardona evaporite horizon, while the depocenter remained approximately stationary (Figure 8b). We have no subsidence records for this phase, but sedimentation in the foreland remained continental (Solsona Formation and equivalents; Figure 3a). In this part of the southern foreland, the youngest preserved sediments (Rupelian) are deformed, suggesting deformation continued until at least ~28 Ma. Shortening in the Central Pyrenees is estimated to have ended around 30 Ma based on Apatite fission track data from the Axial Zone (Fitzgerald et al., 1999) or ~24.7 Ma based on magnetostratigraphic dating of the South Central Unit and its footwall (Meigs et al., 1996).

6. Discussion

6.1. Crustal-Scale Model of Orogenic Evolution

Geodynamic models for the Pyrenees have evolved over the last 30 years, as have estimates of total N-S shortening. Most crustal-scale restorations have focused on the Central Pyrenees along the Ariège ECORS deep seismic line. Using upper crustal imbricates in the Axial Zone and restoring to normal crustal thickness, Muñoz (1992) proposes 147 km of N-S shortening while Beaumont et al. (2000) prefer 165 km over several other possible geometries. More recent reconstructions restore to the pre-orogenic rift system (e.g., Mouthereau et al., 2014; Teixell et al., 2016), most notably integrating the hypothesis that the Iberian and European plates were separated by a zone of exhumed mantle due to Aptian-Cenomanian hyperextension (e.g., Jammes et al., 2009; Lagabrielle et al., 2010). However, the original width of this zone and hence the convergence necessary to subsequently close it are unknown. Proposed widths vary from 15 km in the Western Pyrenees (Teixell et al., 2016) to 50 km of exhumed mantle in the Central Pyrenees (Mouthereau et al., 2014) or several hundred kilometers of oceanic crust (Vissers & Meijer, 2012b). However, deep seismic tomography imaging below the Pyrenees rules out oceanic subduction prior to collision, as no subducted oceanic slab can be identified in the mantle (Chevrot et al., 2014). Using full crustal imbrication, as proposed by Roure et al. (1989), Mouthereau et al. (2014) obtain 92 km of total shortening along the ECORS line, excluding closure of the exhumed mantle domain. This markedly lower value is principally related to a revised shortening estimate for the southern Pyrenees compared to Beaumont et al. (2000). In the Western Pyrenees along ECORS-Arzacq, Teixell (1996, 1998) estimates a total shortening of about 80 km, while more recently, Teixell et al. (2016) propose 99 km along a section 15 km to the east of ECORS-Arzacq, excluding closure of the exhumed mantle domain.

In the Eastern Pyrenees, Vergés et al. (1995) integrate surface geology with the deep structure of the ECORS line projected onto the same section line as this paper. By using the work of Baby et al. (1988) for the northern Pyrenees, assuming imbrication of Iberian upper crust only and subduction of Iberian lower crust, restoring to normal crustal thickness, and integrating estimates of erosion and sedimentation during main orogenic phases, they find a minimum total shortening of 125 km. Vergés and García-Senz (2001) revise the restoration (but not the estimated shortening) by proposing two possible geometries for the rifted crust. We further update this reconstruction by integrating the detailed deformation history presented above (Figure 8) with subsidence (Figure 7), thermochronology (e.g., Metcalf et al., 2009), and deep geophysical data (e.g., Chevrot et al., 2015). This allowed us to build a new and more detailed evolutionary model for the Eastern Pyrenees in four phases, chosen to reflect significant changes in the dynamics of the orogenic system (Figure 10). The main differences compared to Vergés et al. (1995, 2002) and Vergés and García-Senz (2001) are summarized in the following paragraphs.

First, the deep structure of the present day section integrates major lithospheric boundaries identified by recent *P* wave tomography and migration of converted *P* waves along the ECORS line (Chevrot et al., 2014, 2015). Chevrot et al. (2015) identify the interface between the top of the Iberian crust and the European mantle, dipping 20°N. Their Iberian Moho (at 32 km depth) corresponds well with ECORS data, but when projected to our section and aligned along the North Pyrenean Fault, the Moho inflection to dip north at 20° is positioned below the Puig-reig anticline (Figure 10a). This Moho geometry leads to an overthickened Iberian crust ($>$50 km) below the Axial Zone, which can be neither isostatically justified nor volumetrically balanced. We therefore continue the Iberian lower crust northward to an inflection point below the southern Axial Zone (as imaged on the ECORS profile), where it dips 20°N into the mantle. This creates a slight mismatch between the projected Moho and our model, a result of the slightly narrower Axial Zone along our section. The apparent southward thinning of the European crust observed by Chevrot et al. (2015) is integrated into our model.

Second, in line with recent findings, the composite fully restored section (end Santonian; Figure 10e) shows the rifted margins separated by a zone of exhumed mantle. Following Mouthereau et al. (2014), this zone has a hypothetical width of 50 km. However, Macchiavelli et al. (2017) suggest a total convergence of ~135 km in the Eastern Pyrenees, which would result in a ~25 km wide exhumed mantle zone in our restoration. Both widths are compatible with our model. The basins are filled with a syn-rift to post-rift succession that is ~4 km thick above mantle. Following Lagabrielle et al. (2010), we position the metamorphosed syn-rift succession (future Metamorphic Internal Zone) directly above mantle. The geometry of the pre-orogenic extensional fault system is still a matter of much debate as discussed above. Restored geometries on the Iberian plate follow those of Vergés and García-Senz (2001) and Vergés et al. (2002), while the European margin is

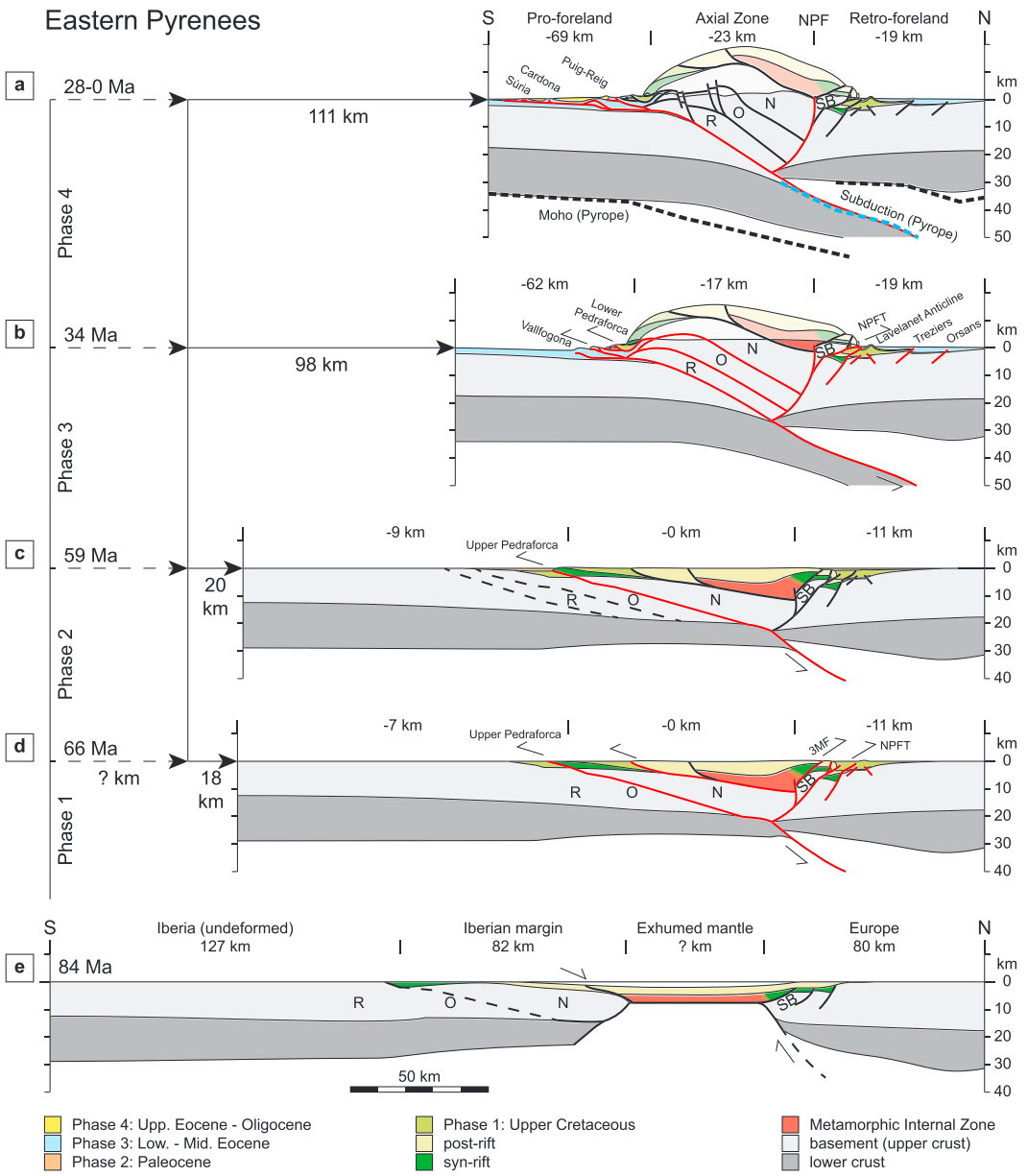

Figure 10. Balanced stepwise evolution of the Eastern Pyrenees. Shortening amounts are cumulative. Red lines indicate faults that have been active since the preceding step. Thick black lines indicate abandoned faults. Dashed lines indicate faults that may have been inherited but have not yet been reactivated. (a) Moho and subduction contact are those along the ECORS line ~50 km to the west, after Chevrot et al. (2015), projected to align along the North Pyrenean Fault. R, Rialp; O, Orri; N, Nogueres; SB, Saint-Barthélémy Massif; NPF, North Pyrenean Fault; 3MF, 3M Fault; NPFT, North Pyrenean Frontal Thrust.

based on new work in this paper. The inferred geometries of the Iberian and European rifted margins are constrained by the observed remnants of extensional Mesozoic basins, preserve the area needed for a precise crustal balancing through time, are isostatically stable, and are guided by new seismic interpretations of the Atlantic Iberian margins (e.g., Sutra et al., 2013).

Third, the lower estimate of shortening for the European plate (~20 km) leads to a new minimum overall shortening of ~111 km. All estimates of shortening given here exclude closure of the exhumed mantle domain. We cannot constrain the original volume of the Metamorphic Internal Zone nor its tectonic and erosional history. The largest uncertainties associated with the amount and distribution of shortening are therefore for the first phase.

6.1.1. First Phase: 84–66 Ma, Rift Inversion

During the Late Cretaceous (Figures 10d and 10e), slow and distributed shortening (~18 km) was accommodated by inversion of normal faults across the whole rift system while the mantle domain closed. An overall shortening rate of ~1 mm/yr is estimated with deformation distributed roughly equally across the two margins (Figures 8b and 8d; Table 1). As this estimate excludes closure of the mantle zone, true convergence rates would be considerably higher. For example, assuming a 50 km wide mantle zone implies a convergence rate of 3.8 mm/yr. The Metamorphic Internal Zone, of unknown dimensions, was thrust northward and probably also southward if we assume that it covered the whole zone of exhumed mantle (Figure 10d; Mouthereau et al., 2014; Teixell et al., 2016). Marine flexural foreland basins developed on both plates and may have formed a continuous basin across the submarine, low relief orogen. Depocenters became overfilled and continental in the Maastrichtian (Figure 3). Average tectonic subsidence rates are 0.09 mm/yr and 0.06 mm/yr for the north and south, respectively. Low-temperature thermochronological data to the east suggest the onset of uplift of the North Pyrenean Massifs during this early phase (Ternois et al., 2017).

6.1.2. Second Phase: 66–59 Ma, Slowdown and Northern Quiescence

The total shortening rate slowed to ~0.4 mm/yr during the Danian and Selandian (Figure 10c). Subduction polarity was established during this phase, the asymmetry of which resulted in a temporary stop in foreland subsidence and deformation of the upper plate (Figures 7d and 8d; Tables 1 and A3). However, very slow tectonic subsidence (0.05 mm/yr) and shortening (0.4 mm/yr) continued on the lower plate, accommodating some 2 km of shortening. Continental sedimentation prevailed in both foreland basins.

6.1.3. Third Phase: 59–34 Ma, Main Collision and Southern Dominance

The principal phase of collision (approximately 78 km of shortening) took place between ~59 and ~34 Ma with shortening and tectonic subsidence rates revealing a strong asymmetry, being much higher in the south (2.7 mm/yr and 0.12 mm/yr on average, respectively) than in the north (0.3 mm/yr and 0.03 mm/yr on average, respectively; Figures 7 and 8; Table 1). The peak in overall shortening rate (~4.5 mm/yr) began at ~56 Ma and was followed by a gradual deceleration to 2.3 mm/yr until ~36 Ma, when accretion of a new basement thrust sheet (Rialp) increased the overall rate to 2.9 mm/yr (Figures 8a and A1c). The South Pyrenean wedge accommodated ~70 km of shortening by frontal accretion and thickening of the Axial Zone. In the north, shortening was accommodated along several thrusts simultaneously, with the North Pyrenean Frontal Thrust accounting for the majority of shortening (Figure 8c). After the early Ypresian marine incursion, continental conditions were quickly re-established in the northern foreland, while the south sustained a carbonate platform and deep marine basin until ~36 Ma (Figure 3; Costa et al., 2010; Vergés et al., 1998). Low-temperature thermochronology records uplift and exhumation of the Axial Zone from ~50 Ma (e.g., Metcalf et al., 2009), which is corroborated by alluvial sedimentation along the thrust fronts of both wedges.

6.1.4. Fourth Phase: 34–28 Ma, Final Shortening

In the final stage, after ~34 Ma, orogenic processes gradually died out. The eastern northern foreland appears to have been abandoned at around 34 Ma, but this is unclear due to later uplift and erosion (Figure 8c; Table 1). In contrast, during the Oligocene, ~13 km of shortening was accommodated in the south by detachment anticlines above the Cardona salt horizon (~7 km) and by internal deformation and uplift of the Axial Zone (~6 km; Figures 8a, 8b, and 10a). While the exact timing of the end of convergence is not well known, we estimate an average shortening rate of ~2.2 mm/yr (Table 1) up to at least ~28 Ma. Post-orogenic exhumation of the southern Axial Zone continued into the Miocene (Rushlow et al., 2013).

6.2. Improved Detail in Orogen Deformation History

Crustal deformation histories previously proposed for the Pyrenees are similar in broad terms to our results, with inversion of the rift followed by pro-wedge propagation and basement stacking in the Axial Zone (e.g., Sinclair et al., 2005). However, along our section in the Eastern Pyrenees, the distribution of displacement on faults through time (Figure 8) has revealed a more detailed deformation history.

While recent models include the closure of an exhumed mantle domain, how this event relates to inversion of the rifted margins remains difficult to constrain. Mouthereau et al. (2014) show the mantle domain closing first, followed by thick-skinned inversion of rift structures after ~75–70 Ma. We propose instead that closure of the mantle domain took place progressively and simultaneously with thick-skinned inversion of the rifted margins, based on timing of the North Pyrenean Frontal Thrust as constrained by stratigraphy. This is corroborated by the foreland tectonic subsidence signal that we link to emplacement of the Metamorphic Internal Zone and loading of the margins.

None of the published crustal-scale restorations recognize the Paleocene slowdown described in this paper, either because it is below the temporal resolution of the sequential restoration steps used (Beaumont et al., 2000; Muñoz, 1992; Teixell et al., 2016) or because it cannot be detected by time-temperature models from apatite fission track data used to constrain vertical motions (Mouthereau et al., 2014). Furthermore, previous attempts at estimating convergence rates through time have given conflicting results. In the Central Pyrenees, Beaumont et al. (2000) show an overall acceleration, in particular at 36 Ma, related to late stacking of crustal thrust sheets in the Axial Zone. In contrast, Mouthereau et al. (2014) propose a high initial rate of convergence (~3 mm/yr) in the Late Cretaceous and early Paleocene, followed by gradual deceleration until the Miocene. For the Western Pyrenees, Teixell et al. (2016) estimate very low rates ($<$1 mm/yr) during the Late Cretaceous and Paleocene, followed by the principal peak of convergence in the Eocene (3–2.5 mm/yr). Along our section in the Eastern Pyrenees, we show three peaks of relatively rapid shortening (83, 56, and 36 Ma), each followed by a period of slower and decelerating shortening (Figures 8b, 8d, and A1; Table 1). We discuss the main differences in the following paragraphs.

The highest shortening rates in the Eastern Pyrenees, according to our reconstruction, occurred during the early Eocene, which can be considered as the onset of main collision. This coincides with relatively rapid tectonic subsidence of the Aquitaine Basin starting at ~55 Ma (Figure 7; Desegaulx & Brunet, 1990; Ford et al., 2016; Rougier et al., 2016) and the onset of crustal stacking in the Axial Zone around 50 Ma (e.g., Metcalf et al., 2009). Teixell et al. (2016) show that the main pulse of shortening in the Western Pyrenees also occurred during the Eocene. In the Central Pyrenees, however, neither Beaumont et al. (2000) nor Mouthereau et al. (2014) place the highest shortening rates during the Eocene. The initial high shortening rate of Mouthereau et al. (2014) is based on Late Cretaceous to Paleocene cooling detected by detrital low-temperature thermochronology, from foreland basin sediments that the authors assume were derived from the Pyrenean orogen. However, paleocurrent and facies analyses (Bilotte, 1985) show that these sediments were sourced from an area to the east of the Pyrenees. Therefore, these data do not constrain exhumation rate in the Pyrenees along the ECORS line. Furthermore, the gradually decelerating convergence proposed by Mouthereau et al. (2014) cannot be reconciled with the increased Eocene tectonic subsidence and shortening rates for the forelands. Beaumont et al. (2000) place the highest shortening rates after 36 Ma, in accordance with rapid exhumation in the Axial Zone, as shown by numerous thermochronological studies (Fillon & van der Beek, 2012; Fitzgerald et al., 1999; Jolivet et al., 2007; Maurel et al., 2008; Metcalf et al., 2009; Morris et al., 1998; Rushlow et al., 2013). However, thrusting along the eastern border of the South Central Unit (~25 km east of ECORS; Figure 1a) appears to have slowed down after 36 Ma (Burbank, Vergés, et al., 1992). Furthermore, foreland tectonic subsidence slows down around 36 Ma in both foreland basins. This is well constrained in the south by magnetostratigraphic dating (Figure 7b; Vergés et al., 1998). However, the final deceleration is less well constrained in the north as rates were already very low and the youngest strata are poorly dated and preserved (Figure 7d; Ford et al., 2016). Although the peak in exhumation rate of the Axial Zone may have occurred around 36 Ma, there is evidence for exhumation of the Axial Zone since ~50 Ma (Fitzgerald et al., 1999; Metcalf et al., 2009; Rahl et al., 2011; Sinclair et al., 2005; Whitchurch et al., 2011). Because exhumation rate cannot be directly related to shortening rate, we assume a constant shortening rate for internal shortening of the Axial Zone since ~50 Ma, thus yielding a lower shortening rate after 36 Ma than shown by Beaumont et al. (2000) and providing a better fit with foreland evolution.

Using fully independent methods and data sources, Macchiavelli et al. (2017) developed a new plate kinematic model for Iberia. The N-S shortening rates between Iberia and Europe predicted by this model are in good agreement with our own results (Figure A1). They predict slow convergence (~0.9 mm/yr) during the Late Cretaceous and Danian, with a minor extension phase in the Selandian and Thanetian. Their model predicts the highest convergence rates in Ypresian and Lutetian times (~3.6 mm/yr), slightly slower convergence during Bartonian and Priabonian times (~2.8 mm/yr), followed by rapid convergence during the Oligocene (~3.9 mm/yr). The good agreement between our results and those obtained from completely independent methods and data (Macchiavelli et al., 2017) shows that our approach gives good results and can be applied to other natural systems to better constrain their evolution.

6.3. Linked Pro- and Retro-Wedge Dynamics

As described in section 6.1, Late Cretaceous shortening was distributed across both the Iberian and European rifted margins, before the convergent system evolved into an asymmetrical, pro-wedge-dominant orogen (Figures 8b and 8d). Models of doubly vergent orogens with distinct lower and upper plates typically show

a pro-wedge-dominant shortening distribution (Beaumont et al., 2000; Cruz et al., 2008; Duerto & McClay, 2009; Erdős et al., 2014, 2015; Hoth et al., 2007; Hardy et al., 2009; Jammes & Huismans, 2012; Jammes, Huismans, & Muñoz, 2014; Sinclair et al., 2005). However, at the onset of Pyrenean convergence, no such distinction can be made. Instead, the template consists of two opposing rifted margins separated by exhumed mantle (Clerc et al., 2015; Jammes et al., 2009, 2014; Lagabrielle et al., 2010; Mouthereau et al., 2014; Vacherat et al., 2016). Numerical models that include rifted margins show early inversion that is roughly symmetrical, until full collision and onset of subduction of continental mantle lithosphere forces a change to an asymmetric geometry at depth (Erdős et al., 2014; Jammes et al., 2014; Jammes & Huismans, 2012). Whether this change to an asymmetric deep geometry in the Pyrenees occurred during closure of the exhumed mantle domain or at the beginning of main collision is unclear. Our model suggests that the transition to a pro-wedge-dominant shortening distribution and related abandonment of the retro-wedge around 66 Ma occurred shortly after closure of the exhumed mantle domain. The change in shortening distribution may thus record the change from early rift inversion to main collision (i.e., continental subduction) in the Pyrenees, implying this major change does not necessarily rely on external forcing. In the Western Pyrenees, Teixell et al. (2016) infer that closure of the mantle domain did not occur until the Early Eocene. This suggests that early convergence was less significant in the west than in the east and/or that the mantle domain was wider in the west than in the east as proposed by Jammes et al. (2009).

The Paleocene retro-foreland quiescence must be explained on a regional scale, as it has also been recognized in the Central Pyrenees (Ford et al., 2016; Rougier et al., 2016). One potential cause for this north Pyrenean quiescence is a pause in plate convergence. While some plate reconstructions based on magnetic sea floor anomalies show a complete stagnation of convergence in the Paleocene (Macchiavelli et al., 2017; Roest & Srivastava, 1991; Rosenbaum et al., 2002), others show continuous convergence (Vissers & Meijer, 2012a). Other potential contributing factors for the north Pyrenean quiescence can be related to the redistribution of shortening within the surrounding plates (e.g., Mouthereau et al., 2014) or a change in the deep structure of the orogen as it evolves to full collision, as discussed below.

Late Cretaceous subsidence in both the pro- and retro-forelands was mainly driven by loading related to emplacement of the Metamorphic Internal Zone and onset of inversion of the rifted margins. Thanetian to Oligocene pro-foreland behavior can be directly related to crustal thickening and loading during main collision. We here propose that contemporaneous retro-foreland subsidence was driven by backthrusting of the thickened pro-wedge onto the European plate, similar to predictions from numerical and analogue models (e.g., Erdős et al., 2014; Hoth et al., 2007). The deep structure imaged by the ECORS line indicates that the northern part of the Axial Zone overlies the European plate (Figure 1b; Muñoz, 1992; Roure et al., 1989; Teixell, 1998; Teixell et al., 2016). Thermochronological data generally place the onset of exhumation in the Axial Zone at ~50 Ma (Fitzgerald et al., 1999; Metcalf et al., 2009; Rahl et al., 2011; Sinclair et al., 2005; Whitchurch et al., 2011), but in the Eastern Pyrenees, this may have started as early as ~55–60 Ma (Maurel et al., 2008). Tectonic subsidence of the retro-foreland resumed around 59 Ma, suggesting that the period between the onset of pro-dominant shortening distribution (~66 Ma) and the onset of Axial Zone backthrusting (~60 Ma at the earliest) may have contributed to the Paleocene quiescence observed in the retro-foreland.

Using subsidence analysis and detailed tectonic reconstructions to compare the evolution on both sides of a natural system has given insight into crustal-scale dynamics of doubly vergent orogens. The shortening distribution between the pro- and retro-wedges is not constant through time. So far, such changes have not been suggested by models (e.g., Hoth et al., 2007; Sinclair et al., 2005). Previous foreland basin subsidence models simplify the orogen into a uniformly growing double wedge and therefore do not predict multiple periods of retro-foreland subsidence nor a quiescent phase (Naylor & Sinclair, 2008; Sinclair et al., 2005; Sinclair & Naylor, 2012). Changes in the shortening distribution over time may be intrinsic to the system and independent of external factors, implying that other inverted rift systems show a similar change in shortening distribution from equal to pro-dominant. This implication requires independent verification, through modeling and comparing with other orogens, which is the subject of a future paper.

7. Conclusions

We present new stratigraphic and tectonic data for the north Pyrenean fold-and-thrust belt and Aquitaine Basin in the Eastern Pyrenees, which, when integrated with published data, provide new insight into retro-

wedge evolution. By integrating these new results with equivalent data on a section through the southern Pyrenees and other published data (thermochronology and seismic tomography data), we derive an updated full crustal history of the East Pyrenean double-wedge orogen.

Calculated minimum shortening for the East Pyrenean retro-wedge and Aquitaine Basin was ~20 km during the Pyrenean orogeny. Late Cretaceous shortening and tectonic subsidence rates in the northern Pyrenees (0.6 mm/yr and 0.09 mm/yr, respectively) were followed by a Paleocene quiescence and lower rates during the Eocene (0.3 mm/yr and 0.03 mm/yr). A minimum overall N-S shortening of ~111 km was estimated for the Eastern Pyrenees, not including closure of an inferred exhumed mantle domain of unknown width.

The evolution of the double wedge orogen is divided into four phases: (1) Late Cretaceous shortening was characterized by closure of the exhumed mantle domain and inversion of the Iberian and European margins. An overall shortening rate of ~1 mm/yr on average was distributed roughly equally between the two margins. Significant early foreland basins developed on both margins well before the creation of significant topography. (2) In the Paleocene, slow shortening continued in the southern Pyrenees (~0.4 mm/yr on average) while the north was temporarily inactive. (3) The highest overall shortening rate was reached in the Eocene (~3.1 mm/yr on average) recording main collision. This was predominantly accommodated by shortening in the southern Pyrenees and Axial Zone. However, continued thickening of the Axial Zone then led to backthrusting onto the upper plate, reactivating the retro-wedge and its foreland basin. (4) Overall shortening slowed in the Oligocene to ~2.1 mm/yr on average. The northern Pyrenees were probably inactive in this phase. According to our revised evolutionary model for the Eastern Pyrenees, the evolution from rift inversion to main collision caused a change from equal shortening in both rifted margins to a pro-wedge dominant shortening distribution, accompanied by a temporary quiescence of the retro-wedge.

Comparative analysis of pro- and retro-wedge behavior reveals the self-organization of a complex orogenic system. Major changes or events (change in strain distribution) may be due to internal thresholds being reached that are intrinsic to inverted rift systems (e.g., onset of continental collision) and therefore may not rely on external forcing (plate kinematics), implying other inverted rift systems may behave similarly. The good agreement between our results and those obtained from fully independent data and methods shows that this detailed approach can be used to further constrain the evolution of other natural systems. We believe that in other orogens, it can potentially identify similar self-organization and intrinsic thresholds involved in orogenesis.

Acknowledgments
This study was funded by the ANR (France) PYRAMID research project. The French-Norwegian Foundation (13-06 PYR-FFTP; sedimentary basin and North Pyrenean foreland fold and thrust belt formation) supported study visits to the University of Bergen, Norway. Collaboration with CSIC Barcelona, Spain was funded by the project ALPIMED (PIE-CSIC-201530E082). A stratigraphic correlation of the BRGM 1:50,000 geological maps supporting Figure is available as Table A1 in the supporting information. Detailed subsidence data supporting Figure are available as Tables A2, A3, and A4 in the supporting information. Field data used to constrain the structure in the northern Pyrenees (Figures 2, 4, 5, and) are available as Table A5 in the supporting information. We thank colleagues at the CRPG and the PYRAMID team, in particular Michel de Saint Blanquat, for fruitful discussions on the structure and nature of the Metamorphic Internal Zone in the Saint-Barthélémy area. We thank Chiara Macchiavelli for providing Pyrenean convergence rates from an early version of her work. We thank Andrew Leier, an anonymous reviewer, and the Editor for their insightful comments that helped to significantly improve the manuscript. This is CRPG contribution no. 2554.

References

Anadón, P. (1986). Las facies lacustres del olioceno de campins (Vallès Oriental, provincia de Barcelona). *Cuadernos de Geología Ibérica*, *10*, 271–294.

Angrand, P., Ford, M., & Watts, A. B. (2018). Lateral variations in foreland flexure of a rifted continental margin: The Aquitaine Basin (SW France). *Tectonics*, *37*. https://doi.org/10.1002/2017TC004670

Ardèvol, L., Klimowitz, J., Malagón, J., & Nagtegaal, P. J. C. (2000). Depositional sequence response to foreland deformation in the Upper Cretaceous of the southern Pyrenees, Spain. *American Association of Petroleum Geologists Bulletin*, *84*(4), 566–588. https://doi.org/10.1306/C9EBCE55-1735-11D7-8645000102C1865D

Baby, P. (1988). Chevauchements dans une zone à structure complexe: La zone nord-pyrénéenne ariégeoise, PhD thesis, Université Paul Sabatier Toulouse III, Toulouse, France.

Baby, P., Crouzet, G., Specht, M., Deramond, J., Bilotte, M., & Debroas, E.-J. (1988). Rôle des paléostructures albo-cénomaniennes dans la géométrie des chevauchements fronaux nord-pyrénéens. *Comptes-rendus de l'Académie des Sciences de Paris*, *306*(2), 307–313.

Beaumont, C., Muñoz, J. A., Hamilton, J., & Fullsack, P. (2000). Factors controlling the Alpine evolution of the Central Pyrenees inferred from a comparison of observations and geodynamical models. *Journal of Geophysical Research*, *105*(B4), 8121–8145. https://doi.org/10.1029/1999JB900390

Bilotte, M. (1985). Le Crétacé supérieur des plates-formes est-pyrénéennes. In *Strata*, (Vol. 5). Toulouse, France: Université Paul-Sabatier.

Bilotte, M., Casteras, M., Peybernès, B., Rey, J., Soula, J.-C., & Taillefer, F. (1988). *Carte géologique de la France au 1/50 000: Foix (feuille Nº1075)*. Orléans, France: BRGM.

Bilotte, M., Cosson, J., Crochet, B., Peybernès, B., Roche, J., Taillefer, F., … Villatte, J. (1988). *Carte géologique de la France au 1/50 000: Lavelanet (feuille Nº1076)*. Orléans, France: BRGM.

Bilotte, M., Cosson, J., Crochet, B., Peybernès, B., Roche, J., Taillefer, F., … Villatte, J. (1988). *Notice explicative de la feuille Lavelanet à 1/50 000 (Feuille Nº1076)*. Orléans, France: BRGM.

Bond, R. M. G., & McClay, K. R. (1995). Inversion of a Lower Cretaceous extensional basin, south central Pyrenees, Spain. In J. G. Buchanan, & P. G. Buchanan (Eds.), *Basin inversion*, *Geological Society Special Publication*, (Vol. 88, pp. 415–431). London, UK: Geological Society of London.

Bulnes, M., & Poblet, J. (1999). Estimating the detachment depth in cross sections involving detachment folds. *Geological Magazine*, *136*(4), 395–412, S0016756899002794. https://doi.org/10.1017/S0016756899002794

Burbank, D. W., Puigdefàbregas, C., & Muñoz, J. A. (1992). The chronology of the Eocene tectonic and stratigraphic development of the eastern Pyrenean foreland basin, northeast Spain. *Geological Society of America Bulletin*, *104*(9), 1101–1120. https://doi.org/10.1130/0016-7606(1992)104%3C1101:TCOTET%3E2.3.CO;2

Burbank, D. W., Vergés, J., Munoz, J. A., & Bentham, P. (1992). Coeval hindward- and forward-imbricating thrusting in the south-central Pyrenees, Spain: Timing and rates of shortening and deposition. *Geological Society of America Bulletin*, *104*(1), 3–17. https://doi.org/10.1130/0016-7606(1992)104%3C0003:CHAFIT%3E2.3.CO;2

Carrigan, J. H., Anastasio, D. J., Kodama, K. P., & Parés, J. M. (2016). Fault-related fold kinematics recorded by terrestrial growth strata, Sant Llorenç de Morunys, Pyrenees Mountains, NE Spain. *Journal of Structural Geology*, *91*, 161–176. https://doi.org/10.1016/j.jsg.2016.09.003

Cavaillé, A. (1976a). *Carte géologique de la France au 1/50 000: Mirepoix (Feuille Nº 1058)*. Orléans, France: BRGM.

Cavaillé, A. (1976b). *Notice explicative de la feuille Mirepoix à 1/50 000 (Feuille Nº1058)*. Orléans, France: BRGM.

Cavaillé, A., Debat, P., & Calas, G. (1975a). *Carte géologique de la France au 1/50 000: Castelnaudary (feuille Nº1036)*. Orléans, France: BRGM.

Cavaillé, A., Debat, P., & Calas, G. (1975b). *Notice explicative de la feuille Castelnaudary à 1/50 000 (Feuille Nº1036)*. Orléans, France: BRGM.

Chevrot, S., Sylvander, M., Diaz, J., Ruiz, M., Paul, A., & the PYROPE Working Group (2015). The Pyrenean architecture as revealed by teleseismic *P*-to-*S* converted waves recorded along two dense transects. *Geophysical Journal International*, *200*(2), 1094–1105. https://doi.org/10.1093/gji/ggu400

Chevrot, S., Villaseñor, A., Sylvander, M., Benahmed, S., Beucler, E., Cougoulat, G., … Wolyniec, D. (2014). High-resolution imaging of the Pyrenees and Massif Central from the data of the PYROPE and IBERARRAY portable array deployments. *Journal of Geophysical Research: Solid Earth*, *119*, 6399–6420. https://doi.org/10.1002/2014JB010953

Choukroune, P. (1974). Structure et evolution tectonique de la zone nord-Pyrénéenne. Analyse de la déformation dans une portion de chaine a schistosité sub-verticale., PhD thesis, Université des Sciences et Techniques du Languedoc, Montpellier, France.

Choukroune, P., & Mattauer, M. (1978). Tectonique des plaques et Pyrénées: sur le fonctionnement de la faille transformante nord-Pyrénéenne; comparaisons avec des modèles actuels. *Bulletin de la Societe Geologique de France*, *7 t. XX*(5), 689–700.

Christophoul, F., Soula, J.-C., Brusset, S., Elibana, B., Roddaz, M., Bessiere, G., & Deramond, J. (2003). Time, place and mode of propagation of foreland basin systems as recorded by the sedimentary fill: Examples of the Late Cretaceous and Eocene retro-foreland basins of the north-eastern Pyrenees. In T. McCann, & A. Saintot (Eds.), *Tracing tectonic deformation using the sedimentary record*, *Geological Society, London, Special Publications* (Vol. 208, pp. 229–252). London, UK: Geological Society of London.

Clerc, C., Lahfid, A., Monié, P., Lagabrielle, Y., Chopin, C., Poujol, M., … de Saint Blanquat, M. (2015). High-temperature metamorphism during extreme thinning of the continental crust: A reappraisal of the north Pyrenean passive paleomargin. *Solid Earth*, *6*(2), 643–668. https://doi.org/10.5194/se-6-643-2015

Cochelin, B., Lemirre, B., Denèle, Y., de Saint Blanquat, M., Lahfid, A., & Duchêne, S. (2017). Structural inheritance in the Central Pyrenees: The Variscan to Alpine tectonometamorphic evolution of the Axial Zone. *Journal of the Geological Society of London*, jgs2017–jgs2066. https://doi.org/10.1144/jgs2017-066

Cohen, K. M., Finney, S., & Gibbard, P. L. (2013). International chronostratigraphic chart 2013/01, International Commision on Stratigraphy.

Costa, E., Garcés, M., López-Blanco, M., Beamud, E., Gómez-Paccard, M., & Larrasoaña, J. C. (2010). Closing and continentalization of the south Pyrenean foreland basin (NE Spain): Magnetochronological constraints. *Basin Research*, *22*(6), 904–917. https://doi.org/10.1111/j.1365-2117.2009.00452.x

Crochet, B. (1991). *Molasses syntectoniques du versant nord des Pyrénées: la série de Palassou*. Orléans, France: BRGM.

Crochet, B., Villatte, J., Tambareau, Y., Bilotte, M., Bousquet, R., Kuhfuss, A., … Paris, J. P. (1989). *Carte géologique de la France au 1/50 000: Quillan (Feuille Nº1077)*. Orléans, France: BRGM.

Cruz, L., Teyssier, C., Perg, L., Take, A., & Fayon, A. (2008). Deformation, exhumation, and topography of experimental doubly-vergent orogenic wedges subjected to asymmetric erosion. *Journal of Structural Geology*, *30*(1), 98–115. https://doi.org/10.1016/j.jsg.2007.10.003

de Saint Blanquat, M., Bajolet, F., Grand'Homme, A., Proietti, A., Zanti, M., Boutin, A., … Labaume, P. (2016). Cretaceous mantle exhumation in the central Pyrenees: New constraints from the peridotites in eastern Ariège (north Pyrenean zone, France). *Comptes Rendus Geoscience*, *348*(3–4), 268–278. https://doi.org/10.1016/j.crte.2015.12.003

de Saint Blanquat, M., Lardeaux, J. M., & Brunel, M. (1990). Petrological arguments for high-temperature extensional deformation in the Pyrenean Variscan crust (Saint Barthélémy Massif, Ariège, France). *Tectonophysics*, *177*(1–3), 245–262. https://doi.org/10.1016/0040-1951(90)90284-F

Debroas, E.-J. (1990). Le flysch noir albo-cénomanien témoin de la structuration albienne à sénonienne de la Zone nord-pyrénéenne en Bigorre (Hautes-Pyrénées, France). *Bulletin de la Societe Geologique de France*, *VI*(2), 273–285. https://doi.org/10.2113/gssgfbull.VI.2.273

Decarlis, A., Maino, M., Dallagiovanna, G., Lualdi, A., Masini, E., Seno, S., & Toscani, G. (2014). Salt tectonics in the SW Alps (Italy-France): From rifting to the inversion of the European continental margin in a context of oblique convergence. *Tectonophysics*, *636*, 293–314. https://doi.org/10.1016/j.tecto.2014.09.003

Desegaulx, P., & Brunet, M.-F. (1990). Tectonic subsidence of the Aquitaine Basin since Cretaceous times. *Bulletin de la Societe Geologique de France*, *VI*(2), 295–306. https://doi.org/10.2113/gssgfbull.VI.2.295

Díaz, J., & Gallart, J. (2009). Crustal structure beneath the Iberian Peninsula and surrounding waters: A new compilation of deep seismic sounding results. *Physics of the Earth and Planetary Interiors*, *173*(1-2), 181–190. https://doi.org/10.1016/j.pepi.2008.11.008

Duerto, L., & McClay, K. R. (2009). The role of syntectonic sedimentation in the evolution of doubly vergent thrust wedges and foreland folds. *Marine and Petroleum Geology*, *26*(7), 1051–1069. https://doi.org/10.1016/j.marpetgeo.2008.07.004

Ellenberger, F., Freytet, P., Plaziat, J., Bessiere, G., Viallard, P., Berger, G.-M., & Marchal, J.-P. (1987). *Carte géologique de la France au 1/50 000: Capendu (Feuille Nº1060)*. Orléans, France: BRGM.

Erdős, Z., Huismans, R. S., & van der Beek, P. (2015). First-order control of syntectonic sedimentation on crustal-scale structure of mountain belts. *Journal of Geophysical Research: Solid Earth*, *120*, 5362–5377. https://doi.org/10.1002/2014JB011785

Erdős, Z., Huismans, R. S., van der Beek, P., & Thieulot, C. (2014). Extensional inheritance and surface processes as controlling factors of mountain belt structure. *Journal of Geophysical Research: Solid Earth*, *119*, 9042–9061. https://doi.org/10.1002/2014JB011408

Ershov, A. V., Brunet, M.-F., Nikishin, A. M., Bolotov, S. N., Nazarevich, B. P., & Korotaev, M. V. (2003). Northern Caucasus basin: Thermal history and synthesis of subsidence models. *Sedimentary Geology*, *156*(1-4), 95–118. https://doi.org/10.1016/S0037-0738(02)00284-1

Fillon, C., Huismans, R. S., van der Beek, P., & Muñoz, J. A. (2013). Syntectonic sedimentation controls on the evolution of the southern Pyrenean fold-and-thrust belt: Inferences from coupled tectonic-surface processes models. *Journal of Geophysical Research: Solid Earth*, *118*, 5665–5680. https://doi.org/10.1002/jgrb.50368

Fillon, C., & van der Beek, P. (2012). Post-orogenic evolution of the southern Pyrenees: Constraints from inverse thermo-kinematic modelling of low-temperature thermochronology data. *Basin Research*, *24*(4), 418–436. https://doi.org/10.1111/j.1365-2117.2011.00533.x

Fitzgerald, P. G., Muñoz, J. A., Coney, P. J., & Baldwin, S. L. (1999). Asymmetric exhumation across the Pyrenean orogen: Implications for the tectonic evolution of a collisional orogen. *Earth and Planetary Science Letters*, *173*(3), 157–170. https://doi.org/10.1016/S0012-821X(99)00225-3

Ford, M., Hemmer, L., Vacherat, A., Gallagher, K., & Christophoul, F. (2016). Retro-wedge foreland basin evolution along the ECORS line, eastern Pyrenees, France. *Journal of the Geological Society of London*, *173*, 419–437. https://doi.org/10.1144/jgs2015-129

Ford, M., Williams, E. A., Artoni, A., Vergés, J., & Hardy, S. (1997). Progressive evolution of a fault-related fold pair from growth strata geometries, Sant Llorenç de Morunys, SE Pyrenees. *Journal of Structural Geology*, *19*(3–4), 413–441. https://doi.org/10.1016/S0191-8141(96)00116-2

García-Castellanos, D., & Larrasoaña, J. C. (2015). Quantifying the post-tectonic topographic evolution of closed basins: The Ebro basin (northeast Iberia). *Geology*, *43*(8), 663–666. https://doi.org/10.1130/G36673.1

García-Castellanos, D., Vergés, J., Gaspar-Escribano, J., & Cloetingh, S. (2003). Interplay between tectonics, climate, and fluvial transport during the Cenozoic evolution of the Ebro Basin (NE Iberia). *Journal of Geophysical Research*, *108*(B7), 2347. https://doi.org/10.1029/2002JB002073.

Golberg, J. M., & Leyreloup, A. F. (1990). High temperature-low pressure Cretaceous metamorphism related to crustal thinning (eastern north Pyrenean zone, France). *Contributions to Mineralogy and Petrology*, *104*(2), 194–207. https://doi.org/10.1007/BF00306443

Gómez-Paccard, M., López-Blanco, M., Costa, E., Garcés, M., Beamud, E., & Larrasoaña, J. C. (2012). Tectonic and climatic controls on the sequential arrangement of an alluvial fan/fan-delta complex (Montserrat, Eocene, Ebro Basin, NE Spain). *Basin Research*, *24*(4), 437–455. https://doi.org/10.1111/j.1365-2117.2011.00532.x

Gouache, C. (2017). Etudes tectono-métamorphiques des brèches de la zone interne métamorphique des Pyrénées ariégeoises., MSc thesis, Université de Lorraine, Nancy, France.

Hardy, S., McClay, K. R., & Muñoz, J. A. (2009). Deformation and fault activity in space and time in high-resolution numerical models of doubly vergent thrust wedges. *Marine and Petroleum Geology*, *26*(2), 232–248. https://doi.org/10.1016/j.marpetgeo.2007.12.003

Hoth, S., Hoffmann-Rothe, A., & Kukowski, N. (2007). Frontal accretion: An internal clock for bivergent wedge deformation and surface uplift. *Journal of Geophysical Research*, *112*, B06408. https://doi.org/10.1029/2006JB004357

Hoth, S., Kukowski, N., & Oncken, O. (2008). Distant effects in bivergent orogenic belts—How retro-wedge erosion triggers resource formation in pro-foreland basins. *Earth and Planetary Science Letters*, *273*(1-2), 28–37. https://doi.org/10.1016/j.epsl.2008.05.033

Jammes, S., & Huismans, R. S. (2012). Structural styles of mountain building: Controls of lithospheric rheologic stratification and extensional inheritance. *Journal of Geophysical Research*, *117*, B10403. https://doi.org/10.1029/2012JB009376

Jammes, S., Huismans, R. S., & Muñoz, J. A. (2014). Lateral variation in structural style of mountain building: Controls of rheological and rift inheritance. *Terra Nova*, *26*(3), 201–207. https://doi.org/10.1111/ter.12087

Jammes, S., Manatschal, G., Lavier, L. L., & Masini, E. (2009). Tectonosedimentary evolution related to extreme crustal thinning ahead of a propagating ocean: Example of the western Pyrenees. *Tectonics*, *28*, TC4012. https://doi.org/10.1029/2008TC002406

Jarvis, A., Reuter, H. I., Nelson, A., & Guevara, E. (2008). Hole-filled SRTM data V4, International Centre for Tropical Agriculture (CIAT). Retrieved from http://srtm.csi.cgiar.org

Jolivet, M., Labaume, P., Monié, P., Brunel, M., Arnaud, N., & Campani, M. (2007). Thermochronology constraints for the propagation sequence of the south Pyrenean basement thrust system (France-Spain). *Tectonics*, *26*, TC5007. https://doi.org/10.1029/2006TC002080

Lagabrielle, Y., Labaume, P., & de Saint Blanquat, M. (2010). Mantle exhumation, crustal denudation, and gravity tectonics during Cretaceous rifting in the Pyrenean realm (SW Europe): Insights from the geological setting of the lherzolite bodies. *Tectonics*, *29*, TC4012. https://doi.org/10.1029/2009TC002588

Laumonier, B. (2015). The alpine southeastern Pyrenees (France, Spain); a synthesis. *Rev. Géologie pyrénéenne*, *2*(1), 44.

Lewis, C. J., Vergés, J., & Marzo, M. (2000). High mountains in a zone of extended crust: Insights into the Neogene-Quaternary topographic development of northeastern Iberia. *Tectonics*, *19*(1), 86–102. https://doi.org/10.1029/1999TC900056

López-Blanco, M., Marzo, M., Burbank, D. W., Vergés, J., Roca, E., Anadón, P., & Piña, J. (2000). Tectonic and climatic controls on the development of foreland fan deltas: Montserrat and Sant Llorenç del Munt systems (middle Eocene, Ebro Basin, NE Spain). *Sedimentary Geology*, *138*(1–4), 17–39. https://doi.org/10.1016/S0037-0738(00)00142-1

Macchiavelli, C., Vergés, J., Schettino, A., Fernàndez, M., Turco, E., Casciello, E., … Tunini, L. (2017). A new southern North Atlantic isochron map: Insights into the drift of the Iberian Plate since the Late Cretaceous. *Journal of Geophysical Research: Solid Earth*, *122*. https://doi.org/10.1002/2017JB014769

Martinez, A., Vergés, J., Clavell, E., & Kennedy, J. (1989). Stratigraphic framework of the thrust geometry and structural inversion in the southeastern Pyrenees: La Garrotxa area. *Geodinamica Acta*, *3*(3), 185–194. https://doi.org/10.1080/09853111.1989.11105185

Marty, F. (1976). Relations géologiques entre le massif du Saint-Barthélémy et les séries post-hercyniennes du pays de Sault (Pyrénées ariégeoises), PhD thesis, Université Paul Sabatier, Toulouse, France.

Maurel, O., Monié, P., Pik, R., Arnaud, N., Brunel, M., & Jolivet, M. (2008). The Meso-Cenozoic thermo-tectonic evolution of the Eastern Pyrenees: An $^{40}Ar/^{39}Ar$ fission track and (U-Th)/He thermochronological study of the Canigou and Mont-Louis massifs. *International Journal of Earth Sciences*, *97*(3), 565–584. https://doi.org/10.1007/s00531-007-0179-x

McClay, K. R., Muñoz, J. A., & García-Senz, J. (2004). Extensional salt tectonics in a contractional orogen: A newly identified tectonic event in the Spanish Pyrenees. *Geology*, *32*(9), 737–740. https://doi.org/10.1130/G20565.1

Meigs, A. J., Vergés, J., & Burbank, D. W. (1996). Ten-million-year history of a thrust sheet. *Bulletin Geological Society of America*, *108*(12), 1608–1625. https://doi.org/10.1130/0016-7606(1996)108%3C1608:TMYHOA%3E2.3.CO;2

Metcalf, J. R., Fitzgerald, P. G., Baldwin, S. L., & Muñoz, J. A. (2009). Thermochronology of a convergent orogen: Constraints on the timing of thrust faulting and subsequent exhumation of the Maladeta Pluton in the Central Pyrenean Axial Zone. *Earth and Planetary Science Letters*, *287*(3-4), 488–503. https://doi.org/10.1016/j.epsl.2009.08.036

Mitra, S., & Mount, V. S. (1998). Foreland basement-involved structures. *American Association of Petroleum Geologists Bulletin*, *82*, 70–109. https://doi.org/10.1306/1D9BC39F-172D-11D7-8645000102C1865D

Morris, R. G., Sinclair, H. D., & Yelland, A. J. (1998). Exhumation of the Pyrenean orogen: Implications for sediment discharge. *Basin Research*, *10*(1), 69–85. https://doi.org/10.1046/j.1365-2117.1998.00053.x

Mouthereau, F., Filleaudeau, P.-Y., Vacherat, A., Pik, R., Lacombe, O., Fellin, M. G., … Masini, E. (2014). Placing limits to shortening evolution in the Pyrenees: Role of margin architecture and implications for the Iberia/Europe convergence. *Tectonics*, *33*, 2283–2314. https://doi.org/10.1002/2014TC003663

Muñoz, J. A. (1992). Evolution of a continental collision belt: ECORS-Pyrenees crustal balanced cross-section. In K. R. McClay (Ed.), *Thrust tectonics* (pp. 235–246). Dordrecht, the Netherlands: Springer.

Naylor, M., & Sinclair, H. D. (2008). Pro- vs. retro-foreland basins. *Basin Research*, *20*(3), 285–303. https://doi.org/10.1111/j.1365-2117.2008.00366.x

Olivet, J. L. (1996). La cinématique de la plaque Ibérique. *Bulletin du Centre de recherches Elf Exploration Production*, *20*, 191–195.

Puigdefàbregas, C., & Souquet, P. (1986). Tecto-sedimentary cycles and depositional sequences of the Mesozoic and Tertiary from the Pyrenees. *Tectonophysics*, *129*(1-4), 173–203. https://doi.org/10.1016/0040-1951(86)90251-9

Pujalte, V., Baceta, J. I., Payros, A., Orue-Etxebarria, X., & Serra-Kiel, J. (1994). Late Cretaceous-middle Eocene sequence stratigraphy and biostratigraphy of the SW and W Pyrenees (Pamplona and Basque basins, Spain), *Libr. des* Excursions du Prem. Congrés Français Stratigr., 1–118.

Rahl, J. M., Haines, S. H., & van der Pluijm, B. A. (2011). Links between orogenic wedge deformation and erosional exhumation: Evidence from illite age analysis of fault rock and detrital thermochronology of syn-tectonic conglomerates in the Spanish Pyrenees. *Earth and Planetary Science Letters*, *307*(1-2), 180–190. https://doi.org/10.1016/j.epsl.2011.04.036

Ramos, E., Busquets, P., & Vergés, J. (2002). Interplay between longitudinal fluvial and transverse alluvial fan systems and growing thrusts in piggyback basin (SE Pyrenees). *Sedimentary Geology*, *146*(1-2), 105–131. https://doi.org/10.1016/S0037-0738(01)00169-5

Reiners, P. W. (2005). Zircon (U-Th)/He thermochronometry. *Reviews in Mineralogy and Geochemistry*, *58*(1), 151–179. https://doi.org/10.2138/rmg.2005.58.6

Ricateau, R., & Villemin, J. (1973). Evolution au Crétacé supérieur de la pente séparant le domaine de plate-forme du sillon sous-pyrénéen en Aquitaine méridionale. *Bulletin de la Societe Geologique de France*, *7*(1), 30–39.

Roest, W. R., & Srivastava, S. P. (1991). Kinematics of the plate boundaries between Eurasia, Iberia, and Africa in the North Atlantic from the Late Cretaceous to the present. *Geology*, *19*(6), 613–616. https://doi.org/10.1130/0091-7613(1991)019%3C0613:KOTPBB%3E2.3.CO;2

Rosenbaum, G., Lister, G. S., & Duboz, C. (2002). Relative motions of Africa, Iberia and Europe during Alpine orogeny. *Tectonophysics*, *359*(1-2), 117–129. https://doi.org/10.1016/S0040-1951(02)00442-0

Rougier, G., Ford, M., Christophoul, F., & Bader, A.-G. (2016). Stratigraphic and tectonic studies in the central Aquitaine Basin, northern Pyrenees: Constraints on the subsidence and deformation history of a retro-foreland basin. *Comptes Rendus Geoscience*, *348*(3-4), 224–235. https://doi.org/10.1016/j.crte.2015.12.005

Roure, F., & Choukroune, P. (1998). Contribution of the ECORS seismic data to the Pyrenean geology: Crustal architecture and geodynamic evolution of the Pyrenees. *Mémoires de la Société Géologique de France*, *173*, 37–52.

Roure, F., Choukroune, P., Berastegui, X., Muñoz, J. A., Villien, A., Matheron, P., … Deramond, J. (1989). ECORS deep seismic data and balanced cross sections: Geometric constraints on the evolution of the Pyrenees. *Tectonics*, *8*(1), 41–50. https://doi.org/10.1029/TC008i001p00041

Rushlow, C. R., Barnes, J. B., Ehlers, T. A., & Vergés, J. (2013). Exhumation of the southern Pyrenean fold-thrust belt (Spain) from orogenic growth to decay. *Tectonics*, *32*, 843–860. https://doi.org/10.1002/tect.20030

Saura, E., Ardèvol, L., Oró, I., Teixell, A., & Vergés, J. (2016). Rising and falling diapirs, shifting depocenters, and flap overturning in the Cretaceous Sopeira and Sant Gervàs subbasins (Ribagorça Basin, southern Pyrenees). *Tectonics*, *35*, 638–662. https://doi.org/10.1002/2015TC004001

Serra-Kiel, J., Canudo, J. I., Dinares, J., Molina, E., Ortiz, N., Pascual, J. O., … Tosquella, J. (1994). Cronoestratigrafía de los sedimentos marinos del Terciario inferior de la Cuenca de Graus-Trem (Zona Central Surpirenaica). *Revista de la Sociedad Geológica de España*, *7*(3–4), 273–295.

Sibuet, J.-C., Srivastava, S. P., & Spakman, W. (2004). Pyrenean orogeny and plate kinematics. *Journal of Geophysical Research*, *109*, B08104. https://doi.org/10.1029/2003JB002514

Sinclair, H. D., Gibson, M., Naylor, M., & Morris, R. G. (2005). Asymmetric growth of the Pyrenees revealed through measurement and modeling of orogenic fluxes. *American Journal of Science*, *305*(5), 369–406. https://doi.org/10.2475/ajs.305.5.369

Sinclair, H. D., & Naylor, M. (2012). Foreland basin subsidence driven by topographic growth versus plate subduction. *Bulletin Geological Society of America*, *124*(3-4), 368–379. https://doi.org/10.1130/B30383.1

Snedden, J. W., & Liu, C. (2010). A compilation of Phanerozoic sea-level change, coastal onlaps and recommended sequence designations, *American Association of Petroleum Geologists Search Discovery*, 40594.

Solé Sugrañes, L., & Clavell, E. (1973). Nota sobre la edad y posición tectónica de los conglomerados eocenos de Queralt (Prepirineo oriental, Prov. de Barcelona). *Acta Geologica Hispánica*, *8*, 1–6.

Souquet, P., & Peybernès, B. (1987). Allochtonie des massifs primaires nord-pyrénéens des Pyrénées Centrales. *Comptes-rendus de l'Académie des Sciences de Paris*, *305*(8), 733–739.

Souquet, P., Peybernès, B., Bilotte, M., & Debroas, E.-J. (1977). La chaîne alpine des Pyrénées. *Géologie de Alpes*, *53*, 193–216.

Souquet, P., Debroas, E.-J., Boirie, J.-M., Pons, P., Fixari, J.-G., Roux, J.-C., … Peybernes, B. (1985). Le groupe du Flysch noir (albo-cénomanien) dans les Pyrénées. *Bulletin du Centre de recherches Elf Exploration Production*, *9*, 183–252.

Souriau, A., Chevrot, S., & Olivera, C. (2008). A new tomographic image of the Pyrenean lithosphere from teleseismic data. *Tectonophysics*, *460*(1–4), 206–214. https://doi.org/10.1016/j.tecto.2008.08.014

Srivastava, S. P., Roest, W. R., Kovacs, L. C., Oakey, G., Lévesque, S., Verhoef, J., & Macnab, R. (1990). Motion of Iberia since the Late Jurassic: Results from detailed aeromagnetic measurements in the Newfoundland Basin. *Tectonophysics*, *184*(3–4), 229–260. https://doi.org/10.1016/0040-1951(90)90442-B

Steckler, M. S., & Watts, A. B. (1978). Subsidence of the Atlantic-type continental margin off New York. *Earth and Planetary Science Letters*, *41*(1), 1–13. https://doi.org/10.1016/0012-821X(78)90036-5

Sutra, E., Manatschal, G., Mohn, G., & Unternehr, P. (2013). Quantification and restoration of extensional deformation along the Western Iberia and Newfoundland rifted margins. *Geochemistry, Geophysics, Geosystems*, *14*, 2575–2597. https://doi.org/10.1002/ggge.20135

Tambareau, Y., Crochet, B., Villatte, J., & Deramond, J. (1995). Evolution tectono-sedimentaire du versant nord des Pyrenees centre-orientales au Paleocene et a l'Eocene inferieur. *Bulletin de la Societe Geologique de France*, *166*(166), 375–387. https://doi.org/10.2113/gssgfbull.166.4.375

Teixell, A. (1996). The Anso transect of the southern Pyrenees: Basement and cover thrust geometries. *Journal of the Geological Society of London*, *153*(2), 301–310. https://doi.org/10.1144/gsjgs.153.2.0301

Teixell, A. (1998). Crustal structure and orogenic material budget in the west central Pyrenees. *Tectonics*, *17*(3), 395–406. https://doi.org/10.1029/98TC00561

Teixell, A., Labaume, P., & Lagabrielle, Y. (2016). The crustal evolution of the west-central Pyrenees revisited: Inferences from a new kinematic scenario. *Comptes Rendus Geoscience*, *348*(3–4), 257–267. https://doi.org/10.1016/j.crte.2015.10.010

Ternois, S., Vacherat, A., Pik, R., Ford, M., & Tibari, B. (2017). Zircon (U-Th)/He evidence for pre-Eocene orogenic exhumation of eastern north Pyrenean massifs, France. In *Geophysical Research Abstracts* (Vol. 19, p. 17649).

Tugend, J., Manatschal, G., Kusznir, N. J., & Masini, E. (2015). Characterizing and identifying structural domains at rifted continental margins: Application to the Bay of Biscay margins and its Western Pyrenean fossil remnants. *Geological Society of London, Special Publication*, *413*(1), 171–203. https://doi.org/10.1144/SP413.3

Vacherat, A., Mouthereau, F., Pik, R., Bellahsen, N., Gautheron, C., Bernet, M., … Radal, J. (2016). Rift-to-collision transition recorded by tectonothermal evolution of the northern Pyrenees. *Tectonics*, *35*, 907–933. https://doi.org/10.1002/2015TC004016

Valero, L., Garcés, M., Cabrera, L., Costa, E., & Sáez, A. (2014). 20 Myr of eccentricity paced lacustrine cycles in the Cenozoic Ebro Basin. *Earth and Planetary Science Letters*, *408*, 183–193. https://doi.org/10.1016/j.epsl.2014.10.007

Vergés, J. (1993). Estudi geològic del vessant sud del Pirineu oriental i central. Evolució cinemàtica en 3D, PhD thesis, University of Barcelona, Spain.

Vergés, J., & Burbank, D. W. (1996). Eocene-Oligocene thrusting and basin configuration in the Eastern and Central Pyrenees (Spain). In P. F. Friend, & C. J. Dabrio (Eds.), *Tertiary basins of Spain. The Stratigraphic Record of Crustal Kinematics* (pp. 120–133). Cambridge, UK: Cambridge University Press. https://doi.org/10.1017/CBO9780511524851.020

Vergés, J., Fernàndez, M., & Martínez, A. (2002). The Pyrenean orogen: Pre-, syn-, and post-collisional evolution. *Journal of the Virtual Explorer*, *08*, 55–74. https://doi.org/10.3809/jvirtex.2002.00058

Vergés, J., & García-Senz, J. (2001). Mesozoic evolution and Cainozoic inversion of the Pyrenean rift. In P. A. Ziegler, et al. (Eds.), *Peri-Tethys Memoir 6: Peri-Tethyan rift/wrench basins and passive margins* (Vol. 186, pp. 187–212). Paris, France: Mémoires du Muséum National d'Histoire Naturelle.

Vergés, J., & Martinez, A. (1988). Corte compensado del Pirineo oriental: Geometría de las cuencas de antepaís y edades de emplazamiento de los mantos de corrimiento. *Acta Geologica Hispánica*, *23*(2), 95–106.

Vergés, J., Martínez-Ríuz, A., Domingo, F., Muñoz, J. A., Losantos, M., Fleta, J., & Gisbert, J. (1994). *Mapa Geológico de España. Plan Magna a escala 1:50 000. Hoja de La Pobla de Lillet (255)*. Madrid, Spain: Instituto Tecnológico Geominero de España.

Vergés, J., Marzo, M., Santaeulària, T., Serra-Kiel, J., Burbank, D. W., Muñoz, J. A., & Giménez-Montsant, J. (1998). Quantified vertical motions and tectonic evolution of the SE Pyrenean foreland basin. In A. Mascle, et al. (Eds.), *Cenozoic foreland basins of western Europe*, *Geological Society Special Publication* (Vol. 134, pp. 107–134). London, UK: Geological Society of London.

Vergés, J., Millán, H., Roca, E., Muñoz, J. A., Marzo, M., Cirés, J., … Cloetingh, S. (1995). Eastern Pyrenees and related foreland basins: Pre-, syn- and post-collisional crustal-scale cross-sections. *Marine and Petroleum Geology*, *12*(8), 903–915. https://doi.org/10.1016/0264-8172(95)98854-X

Vergés, J., Muñoz, J. A., & Martínez, A. (1992). South Pyrenean fold and thrust belt: The role of foreland evaporitic levels in thrust geometry. In K. R. McClay (Ed.), *Thrust tectonics* (pp. 255–264). Dordrecht, The Netherlands: Springer.

Vissers, R. L. M., & Meijer, P. T. (2012a). Iberian plate kinematics and Alpine collision in the Pyrenees. *Earth-Science Reviews*, *114*(1–2), 61–83. https://doi.org/10.1016/j.earscirev.2012.05.001

Vissers, R. L. M., & Meijer, P. T. (2012b). Mesozoic rotation of Iberia: Subduction in the Pyrenees? *Earth-Science Reviews*, *110*(1–4), 93–110. https://doi.org/10.1016/j.earscirev.2011.11.001

Wang, Y., Chevrot, S., Monteiller, V., Komatitsch, D., Mouthereau, F., Manatschal, G., … Martin, R. (2016). The deep roots of the western Pyrenees revealed by full waveform inversion of teleseismic *P* waves. *Geology*, *44*(6), 475–478. https://doi.org/10.1130/G37812.1

Whitchurch, A. L., Carter, A., Sinclair, H. D., Duller, R. A., Whittaker, A. C., & Allen, P. A. (2011). Sediment routing system evolution within a diachronously uplifting orogen: Insights from detrital zircon thermochronological analyses from the south-Central Pyrenees. *American Journal of Science*, *311*(5), 442–482. https://doi.org/10.2475/05.2011.03

Willett, S. D., Beaumont, C., & Fullsack, P. (1993). Mechanical model for the tectonics of doubly vergent compressional orogens. *Geology*, *21*(4), 371–374. https://doi.org/10.1130/0091-7613(1993)021%3C0371:MMFTTO%3E2.3.CO

Woodward, N. B., Boyer, S. E., & Suppe, J. (1989). In M. L. Crawford & E. Padovani (Eds.), *Balanced geological cross-sections: An essential technique in geological research and exploration*. Washington, DC: American Geophysical Union.